

Aged embankment imaging and assessment using surface waves

Author 1

- David Gunn, Ph.D.
- Engineering Geology, British Geological Survey, Nottingham, England

Author 2

- Ben A. J. Dashwood, Ph.D.
- Engineering Geology, British Geological Survey, Nottingham, England

Author 3

- Paolo Bergamo, Ph.D.
- Schweizerischer Erdbebendienst ETH Zurich, Sonneggstrasse 5, 8092 Zurich, Switzerland.

Author 4

- Shane Donohue, Ph.D.
- School of Planning, Architecture and Civil Engineering, Queen's University Belfast, Belfast,
Northern Ireland

Full contact details of corresponding author.

David Gunn, dgu@bgs.ac.uk, Tel: 0115 936 3400

Abstract (150 words)

Rapid, non-intrusive surface wave surveys provide depth profiles from which ground models can be generated for use in earthworks condition assessment. Stiffness throughout earthworks controls behaviour under static and dynamic loads and characterising heterogeneity is of interest in relation to the stability of engineered backfill and life-cycle deterioration in aged utility and transportation infrastructure. Continuous surface wave (CSW) methods were used to identify interfaces between fine and coarse grained fill in an end-tipped embankment along the Great Central Railway in Nottinghamshire. Multichannel analysis of surface wave (MASW) methods were used to characterise subsurface voiding in a canal embankment along the Knottingley and Goole Canal near Eggborough, Yorkshire. MASW methods are currently being used to study the extreme weather impacts upon the stability of a high plasticity clay embankment along the Gloucestershire-Warwickshire Railway near Laverton. Optimal results were obtained using equipment capable of generating and detecting over wide frequency ranges.

Keywords chosen from ICE Publishing list

Embankment; Geophysics; Stiffness; Monitoring; Site Investigation (SI)

List of notation (examples below)

ν	Poisson's Ratio (dimensionless)
V_R	Rayleigh Wave Velocity (ms^{-1})
V_S	Shear Wave Velocity (ms^{-1})
G	Small Strain Stiffness or Shear Modulus (Pa)
ρ_b	Bulk Density (kgm^{-3})
f	Frequency (Hz)
λ_R	Wavelength of Rayleigh Wave (m)
q_c	Cone Penetration Resistance (MPa)
f_s	Sleeve Friction (kPa)
c'	Drained cohesion measured at effective stress (kPa)
ϕ'	Angle of friction at effective stress (degrees $^\circ$)
PL	Moisture content value of the plastic limit (mass ratio convention % g/g)
LL	Moisture content value of the liquid limit (mass ratio convention % g/g)
SI	Site Investigation
.....	
.....	

1. Introduction

1.1 Construction and heterogeneity of aged UK earthworks

Much construction of the UK canal network commenced in the mid-18th century at the beginning of the Industrial Revolution, (Stevenson, 1886). Much railway construction followed in the 19th century, during the formative years of the Industrial Revolution, (Skempton, 1996). The largest concentration of UK canals, roads and railways is in the South East and around the major cities of Birmingham, Leeds, Liverpool and Manchester. Excavation of aged canal and railway cuttings commonly employed large teams of labourers using driven wedges, horse-pulled ploughs, hand tools, and on the later railways such as the Great Central, steam-powered excavators, (Brees 1841, Stevenson 1886, Skempton 1996). While the construction materials were influenced by the underlying geological formations, the engineering characteristics of fine-grained overconsolidated clay or weak mudstone formations favoured relatively easy excavation using these tools, hence, many aged canal and railway earthworks comprise London Clay, Oxford Clay, Gault Clay, Mercia Mudstone and Lias Clay (Reeves *et al.* 2006). The absence of any established practice resulted in embankment construction methods varying considerably between networks, often based upon the experiences of the chief engineer. Side-tipping was commonly employed in the construction of canal embankments and railway embankments were often end-tipped, both using local materials (Skempton, 1996). While modern embankments tend to be structured into well compacted layers, aged embankments often have poor levels of compaction, a greater variability of fill material grades, and usually exhibit highly unique heterogeneity (Selig & Waters, 1994; Skempton, 1996). Earthworks assessment requires the determination of conditions important for the evaluation of performance. Soil type, moisture, stress levels and strength control problems such as plastic deformation, heave, shear failure and mud pumping which lead to a loss of embankment level and support (Perry *et al.* 2003). Surface wave surveys provide a non-invasive means of assessing density and stiffness, which themselves are dependent upon these soil properties, and thus, provide key earthworks condition indicators.

1.2 Embankment characterisation approaches and methods

Repeated visual inspections are mostly used to identify embankment problems, essentially looking for morphological features that confirm movement and anomalous groundwater conditions (Perry *et al.* 2003). This approach is limited, for example because vegetation can often obscure signs of ground movement, subsurface ground and water conditions are not accessible, and slopes often fail 'rapidly' without displaying visible signs of distress. Most common geotechnical monitoring approaches involve displacement measurements of embankments, often following observations of morphological features associated with instability (Dunnicliff 2012). Surface and downhole tilt meters or extensometers are deployed to assess the displacement profile with depth. Such approaches require boreholes and are often accompanied by groundwater level measurements using piezometers. These data inform

stability analyses, aid risk assessments and may contribute to remedial design. These approaches include the expense of intrusive works, and implicitly accept the potential for failure, which does not honour the strict terms of 'early warning'. Indeed, a recent Dept. for Transport (2014) review on infrastructure resilience highlighted the importance of maintaining climate resilient infrastructure and specifically recommended that geotechnical asset owners should "maintain a strong focus on trialling newly available condition monitoring technologies", and improve their "ability to identify and anticipate slopes that will fail and target remedial work as efficiently as possible". Consequently, remotely sensed and non-invasive surface approaches are being explored by many asset owners. Such approaches are better suited for more rapid, cost effective network coverage designed to detect smaller scale changes considered to be the 'pre-cursors' to the morphological features currently used to define marginal condition. Satellite or ground based radar (LiDAR), robotic total stations and photogrammetry provide high resolution ground displacement information (Mazzanti 2012), but still essentially confirm the morphological response to underlying subsurface property (condition) changes that form earlier phases of asset deterioration. With no standard practice and no, or very poor 'as built' documentation, development of conceptual models for predicting the failure modes of aged infrastructure is especially challenging. Geophysical imaging approaches can monitor internal property (condition) changes. These are the precursors connecting surface morphological response to subsurface processes driven by climate and ageing stresses (Gunn et al. 2015a, 2016). These property change signatures offer a potential baseline against which internal condition thresholds can be identified and used as early warning of future instability.

1.3 Embankment characterisation and imaging using surface waves

Penetration into engineered pavements, sub-base and heterogeneous earthworks is especially challenging, and thus, invasive methods can become prohibitively time consuming and costly. Also, while useful for ground truthing, the limited sampling of invasive SI methods makes them unsuitable for imaging irregular heterogeneous structures. Non-invasive geophysical techniques are cost-effective, rapid and may provide 2D and 3D information, which makes them ideal for studying the spatial and temporal variations within assets that cannot be readily captured using discrete boreholes or other forms of geotechnical investigation alone (Chambers *et al.* 2014, Gunn *et al.* 2015a, 2016, Bergamo *et al.* 2016).

Surface wave surveys can be mobilised to image the volumetric distribution of shear wave velocity, and thus, map the small strain stiffness (shear modulus) throughout the earthworks, from which heterogeneity can be assessed (Zagyapan & Fairfield, 2002, Gunn *et al.*, 2013, 2015b, Donohue *et al.*, 2011, Bergamo *et al.*, 2016). These images can be used to assess the unique internal heterogeneity and strength related characteristics arising from the original tipping construction methods, or due to subgrade problems resulting from progressive deterioration. They can inform further site investigation design in relation to poor ground conditions and aid location of more challenging invasive methods such as pitting, cone

penetration resistance testing and coring (Raines *et al.* 2011, Gunn *et al.* 2012). Rayleigh wave analysis, in particular, has been established as a reliable tool for the characterisation of the small strain stiffness (shear modulus, G) of the near surface at the engineering scale (Foti, 2003; Donohue *et al.* 2011, 2013b). Rayleigh waves are dispersive; their phase velocity varies with wavelength and hence, depth of investigation (Socco and Strobbia, 2004). Parametric studies (Xia *et al.*, 1999) have shown the prevailing sensitivity of Rayleigh wave phase velocity to the shear wave velocity structure of the subsurface, so that information on shear modulus distribution can be assessed (Rucker 2003). Also, reasonably short term monitoring programmes by Bergamo *et al.* (2016) indicated distributed variation in Rayleigh wave phase velocity throughout a clay embankment to be sensitive to internal seasonal moisture variations. Such observations indicate the potential for repeat surface wave surveys to be used as a basis for long term asset condition and deterioration monitoring, for example, raising the prospects for condition matrices based directly upon stiffness or its use as a proxy for consolidation, density or saturation. To this end, this paper presents three case histories to demonstrate the application, benefits and limitations of continuous surface wave (CSW) and multi-channel analysis of surface wave (MASW) methods in relation to the assessment of the internal condition of aged embankments. Figure 1 shows the location of the three study sites which include: i. an end-tipped rail embankment in Nottinghamshire, ii. a side-tipped canal embankment in North Yorkshire and iii. a clay rail embankment in Worcestershire.

2. Non-invasive surface wave surveys

2.1 Relevance of surface waves and stiffness to engineering characterisation

Rayleigh waves are often observed as the surface roll resulting from vertical impact on the ground. In fact, two-thirds of the total seismic wave energy generated by such impact propagates as Rayleigh waves (Richart *et al.* 1970, Gunn *et al.* 2012). Rayleigh wave velocity can be derived as a fraction of the shear wave velocity for rocks and soils (Woodward *et al.* 2011), using:

$$V_R = \frac{(0.87+1.12\nu)}{(1+\nu)}V_S \quad 1$$

where ν is Poisson's Ratio. Poisson's ratios for rocks are commonly within the range 0.2 - 0.3. Soils tend to have higher Poisson's ratios around 0.3 - 0.4, which can be even higher in very soft, fully saturated fine grained materials, resulting in Rayleigh wave velocities between 90-95% of shear wave velocities. Shear wave velocity, V_s is controlled by the stiffness, or the small strain shear modulus, G , (Abbis 1981; Hight, *et al.* 1997), and the bulk density, ρ_b , of the medium, given as:

$$V_s = \sqrt{\frac{G}{\rho_b}} \quad 2$$

The bulk density of the soil is the volumetric sum of the densities of the solid soil particles, pore water and the unsaturated air voids. The contribution of the air component is negligible because of its very low density, but porosity and saturation exert very significant control over both bulk density and stiffness of soils and engineered fill (Gunn *et al.* 2003; Donohue *et al.* 2013a). Stiffness is defined as the ratio of stress to strain in material undergoing deformation. Many soils exhibit viscoelastic behaviour leading to strain softening (Bardet 1992), which results in the absolute values of stiffnesses at small strains ($< 10^{-3}$) generally being far greater than at larger strains. For fully saturated soils, porosity, bulk density and inter-particle friction are interrelated with the way in which a soil consolidates, and thus have a very significant influence upon its stiffness and shear wave velocity (Gunn *et al.* 2003). Hardin & Richart (1963) and Richart (1970) showed stiffness to be linearly dependent upon voids ratio for uncemented sands and Viggiani & Atkinson (1995) showed broad linear dependence of clay stiffness to the overconsolidation ratio. In partially saturated soils, there is an additional contribution to stiffness from suctions, which Whalley *et al.* (2012) related to net stress and the matric potential, and Cosentini & Foti (2014) related to soil porosity and saturation using the van Genuchten equation.

2.2 Development of practice and modern surface wave survey field methods

Early procedures using surface Rayleigh wave techniques for soil property testing were suggested in the 1950s, e.g. Jones (1958), but were limited by the technology then available. The procedure, called the steady state Rayleigh method (Jones, 1958; Richart *et al.*, 1970; Rix 1988) used a vertically-acting sinusoidal vibrator, working at a frequency, (f), placed on the ground surface and vertical receivers also on the ground surface, as shown in Figure 2a. Receiver pairs were moved to locations away from the vibrator until the signals measured by them were in phase. At these positions the distance between the receiver pairs was equivalent to the Rayleigh wavelength, λ_R at that particular frequency. The phase velocity of the Rayleigh surface waves was determined using the relationship,

$$V_R = f \times \lambda_R \quad 3$$

By changing the frequency, it is possible to construct a phase velocity – wavelength curve, also known as a Rayleigh wave dispersion curve (V_R vs. λ_R ; or V_S vs. λ_R via Eq. 1). Our surveys included Continuous Surface Wave (CSW) methods, which are a variant of the steady state Rayleigh method. CSW also utilises a controlled frequency, vertical oscillator and a small number of low frequency geophones, Figure 2b. But in this case, the receiver positions remain fixed and the wavelength at each frequency was calculated from the phase differences, $\Delta\phi$ between the ground motions on successive geophones and the spacing, L between them (Joh 1996, Menzies 2001) using:

$$\lambda_R = (L \times \Delta\phi) / (2\pi) \quad 4$$

Joh (1996) suggested wavelengths as short as one third the shortest receiver spacing and as long as three times the largest receiver spacing could be measured with CSW. The range of

wavelengths propagated (V_R/f from Eq. 3) is anticipated for many sites to be from 0.38 m (minimum velocity 75 ms^{-1} at maximum frequency 200 Hz) to 60 m (maximum velocity 300 ms^{-1} at minimum frequency 5 Hz).

Multi-channel Analysis of Surface Waves (MASW) can be performed on the data gathered using the same receiver array configuration adopted in shallow seismic refraction and reflection surveying (Park *et al.*, 1999), Figure 2c. Our MASW surveys employed impulsive sources capable of providing a broad range of frequencies. Source energy was provided by hammer and plate, where higher frequency ranges are produced by lighter sources. Again, velocity dispersion curves are extracted from the phase delays of the different frequency components of the source signal recorded by the receiver array (Park *et al.* 1999; Rucker 2003). MASW surveys were undertaken along profiles running parallel to the axis of embankments. Where static arrays were used, they comprised 24 - 48 vertically polarized geophones, spaced at 0.5 m or 1 m. Longer section coverage was achieved by pulling along and re-locating each successive geophone array to overlap with the previous array that was recorded. Where land streamers were used (Figure 2d), these comprised a 24 channel array of vertically polarised geophones that were mounted on small steel plates, which were towed between intervals equivalent to the shot spacing.

2.3 Shear wave velocity and stiffness profiles and sections

In both MASW and CSW methods the field dispersion curves were inverted to produce a velocity-depth profile for the shallow subsurface (Joh 1996, Foti 2003). The profile was referenced to the centre of the geophone array sub-group, whose records are used to construct the dispersion curve, which could include around 4 geophones for CSW and from around 8 to 12, or even 24 geophones for MASW, Figure 3a, b. The dispersion curve was interactively forward-modelled, which involves ground model inversion and generation of an associated modelled dispersion curve with the best fit to the field curve to determine the subsurface shear-wave velocity profile (Joh 1996, Foti 2003 & Raines *et al.* 2011). The simplest method is attribution of a factored shear wave velocity (usually 1.1 times Rayleigh wave velocity) to a depth equivalent to a fraction of the Rayleigh wavelength, λ_R (Joh 1996, Foti 2003), Figure 3c, d. A factor of $\lambda_R/3$ is most commonly used because a significant proportion of the particle motion in the ground associated with Rayleigh wave propagation is approximately at this depth (Richart *et al.*, 1970; Joh, 1996; Gunn *et al.*, 2006.). The small strain stiffness is the product of the square of the shear wave velocity and the bulk density. The mean (and standard deviation) of 19 bulk density determinations on core from 0.8 m to 5.2 m depths within the embankment fill was 2.01 Mgm^{-3} (0.33 Mgm^{-3}) (Gunn *et al.* 2011), whereas velocity variation ranged from approximately 150ms^{-1} - 250ms^{-1} ; over a 60% variation. Because the stiffness is sensitive to the square of velocity, the bulk density at all depths can be represented by 2.0 Mgm^{-3} , with little effect on the stiffness distribution. On this basis, the stiffness-depth profile was estimated from the shear wave velocity-depth profile. 2D sections were constructed by contour infilling using

anisotropic inverse distance weighting over a grid between each of the shear wave velocity-depth profiles (Gunn et al. 2011, 2013). Also, where MASW surveys were undertaken along a series of parallel arrays, the same weighting method was used to infill grids between the parallel sections to produce a pseudo-3D model of the embankment. (The models were constructed using array parallel surface wave propagation only. More complete 3D models would require surveys across further orthogonally orientated arrays, which are often impractical due to limited crest width across most embankments).

3. Case histories

3.1 Great Central Railway Embankment, East Leake, Nottinghamshire

CSW and MASW surveys were undertaken along a 140 m section of an embankment on the Great Central Railway (GCR) that runs south of the overbridge at East Leake, Nottinghamshire to the East Leake tunnel that passes under the A6006. The whole embankment extends 800 m and was constructed in 1897 using end-tipped materials excavated from adjacent cuttings to the SW and the NE (Bidder, 1900). The railway is operated as a branch from the mainline taking heavy freight class 66 locomotives pulling wagons loaded with supplies for the British Gypsum works at East Leake. Track geometry is very poor due to dipping points and pronounced lateral and vertical warping. Figure 4a shows the layout CSW survey stations relative to the line of MASW surveys that were undertaken using a series of static arrays with a 1 m geophone spacing. Stiffness-depth logs were generated at a series of locations using both methods and ground model was created via grid infill between each depth log, Figures 4b.

Interpretation of the 2D section through the embankment (Figure 4b) includes a basal, high stiffness zone below 5 m depth associated with the underlying Branscombe Mudstone Formation bedrock and an extensive low stiffness zone in the upper 5 m interval associated with the engineered fill of the embankment. Within this upper zone, a prominent high stiffness feature appears between chainage 60 m to 100 m. Whilst in the shallow subsurface between 60 m to 80 m, this feature is related to the ballast, from 80 m to 100 m it is associated with a deeper lens extending to the top of the Branscombe bedrock. This lens appears to be associated with infillings of high stiffness materials including locally sourced sand, gravel and siltstone. Visualisation of the morphology of the high stiffness feature across the embankment in 3D enables a fuller understanding of the spatial context of the structure in relation to the end-tipping construction technique, Figure 5. Core samples from boreholes through the embankment proved fill source material from local cuttings immediately SW and NE of the embankment. Fill materials to the SW of the small stream include Westbury Mudstone that has degraded to soft clay, siltstone of the Blue Anchor Formation (also degraded to clay in places) from the cutting to the SW, and glaciofluvial sand and gravel, thought to be a later infill from local quarries (Bidder, 1900). Clays from the Westbury Formation have stiffnesses ranging from 40 MPa – 80 MPa, whereas the Blue Anchor siltstone and the glaciofluvial sands and gravels tend to be associated with stiffnesses greater than 80 MPa (Gunn *et al.* 2013). Figure 5b shows

stiffnesses from 80 MPa to 120 MPa, i.e. effectively removing the clays of the Westbury Mudstone and also revealing the original ground surface on which the embankment was tipped. Limiting the stiffness ranges enables a domain or anatomical visualisation of morphology, such as the high stiffness structure (from 60 m – 100 m) dominated by Blue Anchor siltstone and glaciofluvial sand and gravel fill. We believe this feature resulted from end tipping as larger boulders ran downslope to the toe of the advancing embankment to be later infilled by finer materials. The engineer in charge of works, Bidder (1900) does not explicitly describe the East Leake embankment construction, but photographs by S.W.A. Newton show end tipping wagons of the contractor, Henry Lovatt at the East Leake tunnel cutting, which is consistent with the ‘cut and fill’ methods used at the time (Leicestershire County Council).

3.2 Knottingley and Goole Canal Embankment, Eggborough, North Yorkshire

The study site was a section of embankment, approximately 450 m W-NW of Whitley Bridge near Eggborough, in the Selby district of North Yorkshire. The embankment, constructed in 1821, forms the retaining barrier on the southern side of the canal, which is raised above the surrounding land by approximately 1.75 m. The site is within a section of the embankment, which is lined on the water side by a vertical masonry wall made of large gritstone ashlar. Parts of the masonry-lined section of the embankment have shown a history of void formation and leakage, resulting in localised partial collapse of the embankment. A series of surface openings were observed during visual inspections in September 2008. One of the prominent features was a collapsed cavity showing significant water seepage at its base. The surface opening appeared to be approximately oval, 1 m by 0.7 m. The subsurface cavity appeared to be funnel-shaped, decreasing in diameter with depth, but extending to 1 m or deeper. It is suspected that the masonry wall was originally lined with puddle clay and the embankment to have been side tipped against the wall. The water appears to have breached the puddle clay seal, entered the north side of the cavity at a depth of around 0.75 m and to have flowed in a south westerly direction deeper into the embankment.

A complete MASW survey was undertaken along four transects, each running parallel to the line of the canal, but offset from the masonry wall by 2 m to 4 m, see Figure 6. Each line was 17.5 m long, comprising 36 channels of vertically polarized geophones spaced at 0.5 m. Embankment geomorphology and survey lines were positioned within a local and BNG coordinate grids using a Leica SmartRover GPS system. GPS points were at 0.5 m along the axis of the embankment and 1 m across the flank. Source locations included an end line offset of 4 m, an end line location and locations within the line spaced at 4 m intervals to enable clearly defined pulses with high signal-noise ratios to be identified on the field traces of the nearby sub-groups of geophones. This was done to guard against the loss of high frequency energy, which is highly attenuated in heterogeneous or disturbed ground.

A 3D ground model was constructed via weighted infill of a grid between each of the shear wave velocity profiles created along a series of overlapping 8-channel geophone groups along each survey line, Figure 6. The aerial extent of the model extends 16 m along the axis and 2 m across the transect of the embankment, approximately centred on the surface void; the depth interval from 0.5 m to 3 m below the embankment crest. The model includes velocities in the range from 85 ms^{-1} to 165 ms^{-1} . The broad characteristics of soils associated with velocities in the range $85 - 100 \text{ ms}^{-1}$ can be considered as loose (low packing density) coarse grained or poorly compacted, very soft or soft fine grained soils (possibly of strengths $<40 \text{ kPa}$) (Hardin & Richart 1963, Richart *et al.* 1970, Gunn *et al.* 2003). Whereas, the broad characteristics of soils associated with velocities in the range $140 - 165 \text{ ms}^{-1}$ can be considered as medium-dense, coarse grained or firm, fine grained soils (possibly of strengths $>75 \text{ kPa}$). Thus, the contours within this soil classification indicate an overall wedge of lower velocity, more poorly compacted, lower strength material thickening towards the east (lower x-axis values) – shown as the darker zones in Figure 6. Within this wedge, two near surface very low velocity ($85 \text{ ms}^{-1} - 90 \text{ ms}^{-1}$) zones occur, where one coincides with the open cavity. A higher velocity ($>130 \text{ ms}^{-1}$), higher strength, stiff basal zone occurs deeper into the section, which we suspect would coincide with the base of the embankment or the top of the underlying superficial geology.

The boundary between the stiffer base (i.e. shear wave velocity $> 130 \text{ ms}^{-1}$) and the overlying weaker soils undulates with a series of marked peaks and troughs, which we suspect provide a subsurface channel for ground water escaping from the canal to drain into the embankment and formation. Progressively removing ground with velocities below 120 ms^{-1} from the 3D model reveals a trough that appears spatially coincident with the flow of water into a subsurface pipe observed from a view into the void, Figure 7. (This observation was made from a position equivalent to $x = 8 \text{ m}$, $y = 1 \text{ m}$ on the local survey grid). We suspect that this trough is formed in stiff sandy, silty clay, where overlying, looser, less cohesive materials were removed by water flowing into this zone via a breach in the canal wall and puddle clay seal. At site, water was observed in video recordings to enter the subsurface pipe from the north, at approximately 0.75 m deep and at $x \cong 8.5 \text{ m}$ along the section. We suspect that the wall and embankment were breached further to the east and that the water followed within the low velocity interval ($< 90 \text{ ms}^{-1}$) between 0.5 m to 1 m deep and between $x = 7 \text{ m}$ to 8 m seen in sections $y = 0 \text{ m}$ to 0.5 m in Figure 7.

3.3 Laverton Railway Embankment, Worcestershire

The Laverton embankment marks the point of a halt in the trains on the current heritage Gloucester and Warwickshire Railway. The line was originally part of the Great Western Railway's Cheltenham–Stratford-upon-Avon–Birmingham line, known as the Honeybourne Line, built between 1900 and 1906. The Laverton embankment is around 6 m high and is believed to have been constructed via end tipping of local Charmouth Mudstone. Currently the

embankment comprises a 0.9 m thick upper layer of ballast fouled with fines, ash and soil (rich in humus), generally underlain by clay fill of reworked Charmouth Mudstone of about 5 m high. The pits at CPT3 and CPT4 (see Figure 8) revealed a layer of cobbles (usually of 100 mm – 250 mm dimensions) at the base of the ballast that would have been laid as part of the original engineered subgrade, as shown in Figure 9. Figure 8a shows the location of repeat MASW surveys that were undertaken at 2 month intervals using a 24-channel land streamer with 4.5 Hz geophones spaced at 1 m. Each time, a 300 m long survey line was completed as a series of 50 increments each of 6 m, where in each case Rayleigh waves were generated by a hammer / plate source offset 2 m from the nearest geophone (Figure 2d). A dispersion curve was generated for each source-line location and an associated shear wave velocity profile plotted at the mid-point of the 24-geophone array. A 2D section was generated from each survey by infilling a grid between each velocity profile, Figure 8b.

The SSW half of the section of the embankment may have been constructed in two lifts, possibly with the boundary at about 3 m depth. Generally, the upper interval exhibits very low penetration resistances of around 1 MPa, while the fill between 3 – 5 m exhibits slight greater penetration resistances (1.3 MPa). Sampling of the clay immediately beneath the ballast around CPT 3 indicated high levels of moisture and weathering. Overall, the corresponding shear wave velocity ranges in the SSW half (0 to CPT 6 at station 180 m) of the section are 80 - 90 ms⁻¹ around 1 m; 100 – 120 ms⁻¹ around 1.5 m; 140 – 150 ms⁻¹ around 3 m and up to 180 ms⁻¹ around 5 m depths. The shear wave velocity section indicates an apparent stiffening of the mid and basal zones of the NNE half of the embankment. The CPT 9 log indicates a thinning of the low penetration resistance interval beneath 1 m interval of ballast, e.g. to around 0.5 m thick. Beneath this, penetration resistances within the interval from 1.5 – 4 m are above 2 MPa, where the associated shear wave velocities are around 140-160 ms⁻¹. This change in the geotechnical properties may relate to increased trafficking or use of different materials in the NNE half of the section approaching the drainage culvert.

Figure 10a shows section of the cone penetration resistance, q_c across the embankment located close to the location of CPT 3 in Figure 8a. The embankment and the weathered zone of the underlying formation can readily be distinguished from the unweathered formation. Values up to 1 MPa are present in the upper interval to around 2.5 m deep below the crest and in the upper 1 m over the East flank. Values within the lower interval (3-5 m) of the embankment range from 1 to 2 MPa. Values in the formation increase from around 2 MPa in the upper 1m of weathered material to above 4 MPa in the unweathered Charmouth. Core logs from a borehole at CPT3 indicate relatively high moisture content levels and low densities throughout the embankment fill, Figure 10b. The density log shows a slight increase in density with depth with a mean bulk density through the embankment of 1.92 Mg.m⁻³, which is below the median value for bulk density of samples gathered from in situ outcrops in the Worcester Basin reported by Hobbs *et al.* (2012), (see Table 1). Relatively low densities are consistent with fill of reworked

material, for example, a consequence of the cut-fill construction method and subsequent ageing processes such as, shrink-swell and fissure development associated with seasonal moisture cycling. Testing on unweathered in situ Charmouth Mudstone sampled from outcrops in the Worcester Basin around Laverton by Hobbs *et al.* (2012) provided values for drained cohesion, c' and friction angle, ϕ' of 19 kPa and 26° , see Table 1. Equivalent test values on re-compacted auger samples recovered from shallow depths were 11.3 kPa and 19.3° from the East flank, where values of 7.3 kPa and 16.2° from the West flank appear to be very close to residual. So, it is likely that fill close to residual strength occurs within a shallow interval (upper 0.5 – 1 m) across the flanks and also the upper interval just underlying ash beneath the rails. Atterberg index tests on the fill materials augered from the upper 0.5m on the East and West flanks indicated plastic (PL) and liquid (LL) limits within the ranges 27-37 % and 61 – 77%. Moisture levels over several intervals through the fill are within this PL range, which is considerably greater than the natural in situ PL of 23%, Figure 10b. Because of its high moisture state the fill consistency here is low. It is likely to be low throughout the zones of low shear wave velocity from CPT 1 to CPT 5 and also around CPT 6, showing how the surface wave image can potentially identify parts of the embankment that are more susceptible to plastic deformation and potentially, shear failure. Around CPT 3, morphological features including a mid-slope berm with lower slope bulging provide evidence of progressive deformation. Backscarp, accumulation and run out zones from a former slip occur above a widened embankment between CPT 5 and 6, which is either the original slipped material or added toe support. Combined moisture content logging and repeat MASW surveys by Bergamo *et al.* (2016) showed a dependence of V_s on the moisture content within the embankment core. In Figure 11, the sequence of sections between CPT 2 and CPT 5 captured during 2014 indicate velocity changes respond very dynamically to weather events. The lowest velocities ($< 110\text{ms}^{-1}$) occur in the upper 3 m over the SSW half of the section between CPT 2 and CPT 3, where very soft clay fill was observed. While velocities are greater (up to 130ms^{-1}) in the NNE half between CPT 4 and CPT 5, larger velocity changes also occur here. Notable are the surveys in Jan 14 within a period of heavy rain and Sept 14 within a relatively dry spell. These sections provide some insight into the possible end-member conditions, e.g. that could be potential trigger points to inspect the embankment for evidence of either very wet or very dry fissured near surface fill. Currently, progressive deterioration in shear strength can only be inferred from repeat V_s surveys. However, quantitative condition assessment is a real possibility in the near term provided robust relationships between shear strength, stiffness and shear wave velocity can be established.

4. Conclusions

CSW and MASW surface wave surveying provide rapid, portable and non-intrusive tools to assess the small strain stiffness characteristics of the railway subgrade and embankment fill. Information is provided in the form of a stiffness profile that provides a useful input into models to characterize the subgrade response to static and dynamic loads. Survey measurements are

repeatable, making these methods very suitable to assess the efficacy of retrospective stiffening of the subgrade such as by vibro-tamping, soil nailing or chemical treatment, such as shown in the case histories by Moxhay et al. (2001, 2008). In the above case histories, signal frequencies up to 200 Hz were measurable with the CSW whereas the MASW was often limited to frequencies below 100 Hz. Signal frequency limitations can occur in the MASW method when using heavier source hammers or long offset distances, but these can be readily overcome by using lighter sources at closer offsets or using high frequencies with a CSW method. Impulsive sources are more convenient and combined with spectral processing yield results far more rapidly than continuous frequency approaches such as used in CSW surveys. Thus, provided a source or sources can be used to generate a relatively wide frequency band (e.g. 5 – 100 Hz), a MASW survey will provide more effective ground coverage. Simple MASW survey field procedures to guard against 'far offset' effects include the use of a constant source–nearest receiver distance and roll-along receiver array relocation to extend lateral coverage.

Like most non-invasive geophysical imaging methods, MASW arrays can be scaled to capture complex structures within aged geotechnical assets. The case histories demonstrate that heterogeneity of aged earthworks structures is not consistent with uniform, laterally extending horizontal layers. 2D sections can be built up from a series of inline velocity–depth profiles spaced at intervals suitable for capturing the heterogeneity even on a sub-metric level. Pseudo 3D sections can be constructed using a series of CSW surveys or using an MASW approach with overlapping gathers of selected channels in subgroups of geophones from larger geophone arrays. Heterogeneous structure related to original construction or, the effect on strength related properties of subsequent localised deterioration within the asset can be located on high resolution Vs or stiffness images. Anatomical imaging is possible, including the location of stiffness contrasts between different engineering materials, understanding dynamic load performance and early identification of progressive subgrade deterioration that precedes track problems or slope failure.

5. Practical Relevance and Potential Applications

Avoidance of the costs associated with service and business disruptions provide compelling cases for early interventions; stated simply by Glendinning et al. (2015) as 'emergency repairs cost 10 times that of planned works'. 'Early' is about when to intervene, or when to act, which depends on the definition of earthworks condition, and the subsequent problems and solutions. The metrics used to define condition are very dependent upon the monitoring approaches and associated technologies. Table 2 maps typical monitoring methods onto the asset management spectrum showing how a progressive transition from responsive to preventative practice involves a shift from the surface to the subsurface. Current practice, such as the example literature in Table 2, largely involves monitoring changes in conditions or properties that precede the morphological signs that generally trigger decisions to monitor movement or

deformation. Technologies to monitor condition cover a range of scales, from a sensor detecting a property time series variation at point, (or at least small volume), to non-invasive geophysical imaging methods that can provide whole asset property variations, in both space and time, potentially enabling holistic (or anatomical) condition assessment. Currently, such images inform further invasive investigation, but with increased acceptance they could also inform design and monitor efficacy of more sophisticated, customised interventions. Improved understanding and quantification of the relationship of seismic properties (G , V_s , ρ) to engineering properties would increase acceptability and use of surface wave surveys. Early focus should include the control of moisture content on both matrix and clast supported fill, for example mapping seismic properties onto consistency, and identifying threshold values of G and V_s associated with critical shrinkage, plastic and liquid limits of fine-grained materials (of various plasticities). The contribution of suction to undrained shear strength also requires further study, especially to quantify its relationship to G and V_s and their sensitivity to saturation, such as from seasonal moisture cycling. Convincing and timely delivery of this information from the research community to the geotechnical asset owners would stimulate the take up of surface wave surveys as part of routine monitoring and management practice.

Acknowledgements

This paper is published with the permission of the Executive Director of the British Geological Survey (NERC). The authors gratefully acknowledge the work of Richard and William Tinsley of Surface Waves Surveys Ltd. who gathered the CSW field data. We also gratefully acknowledge the Great Central Railway (Nottingham) Ltd., the Canal and River Trust and the Gloucester and Warwickshire Railway for allowing access on to the East Leake, Eggborough and Laverton embankments respectively.

References

- Abbiss, C.P. (1981). Shear wave measurements of the elasticity of the ground. *Geotechnique*, 31, (1), 91-104.
- Abdoun, T., Bennett, V., Desrosiers, T. et al. (2013) Asset Management and Safety Assessment of Levees and Earthen Dams Through Comprehensive Real-Time Field Monitoring. *Geotechnical and Geological Engineering*, 31(3), 833-843.
- Bardet, J.P., 1992. A Viscoelastic Model for the Dynamic Behavior of Saturated Poroelastic Soils. *J. App. Mech.* 59, (1), 128-135
- Bemis SP, Micklethwaite S, Turner D, et al. (2014) Ground-based and UAV-Based photogrammetry: A multi-scale, high-resolution mapping tool for structural geology and paleoseismology. *J Struct Geol* 69:163–178.
- Bergamo, P. et al. 2016. Time-lapse monitoring of climate effects on earthworks using surface waves. *Geophysics* 81, (2), 1-15.

- Bidder, F.W., 1900. The Great Central Railway Extension: Northern Division. ICE, Vol. CXLII, Session 1899-1900. Part IV, Paper 3227, 1-22.
- Brees, S.C., 1841. A glossary of civil engineering comprising its theory and modern practice. London, Tilt and Bogue, 310p.
- British Standards Institute: BS 1377: Pt 1: 1990: British Standard Methods of test for soils for civil engineering purposes. Pt 2: Classification tests. Pt 8: Shear strength tests (effective stress).
- Chambers, J., Gunn, D., Wilkinson, P. B., et al. (2014) 4D electrical resistivity tomography monitoring of soil moisture dynamics in an operational railway embankment. *Near Surface Geophysics*, 12, 61-72
- Cosentini, R.M & Foti, S., 2014. Evaluation of porosity and degree of saturation from seismic and electrical data. *Geotechnique*, 64, (4), 278-286
- Dixon, N., Smith, A., Spriggs, M. P., Ridley, A., Meldrum, P. & Haslam, E. (2015). Stability monitoring of a rail slope using acoustic emission. *Proceedings of the Institution of Civil Engineers – Geotechnical Engineering*.
- Donohue, S., Gavin, K. and Tolooiyan., A. (2011). Geophysical and geotechnical assessment of a railway embankment failure, *Near Surface Geophysics*, 9 (1),pp. 33-44.
- Donohue, S. et al. 2013a. Detection of soil compaction using seismic surface waves. *Soil & Tillage Res.* 128, 54-60.
- Donohue, S., Gavin, K. & Tolooiyan, A. 2013b. Railway earthwork stability assessment using geophysics. *Geotechnical and Geophysical Site Characterization*. 4, Vols I and II, 1519-1525.
- Dunnicliff, J. 2012. Chapter 95; Types of geotechnical instrumentation and their usage. In: Burland, J. et al. Ed. ICE manual of geotechnical engineering. ICE, London, 1379-1403.
- Foti S., 2003. Small strain stiffness and damping ratio of Pisa clay from surface wave tests. In: *Geotechnique*, **53**, 455-461.
- Glendinning, S. et al. 2015. Research-informed design, management and maintenance of infrastructure slopes: development of a multi-scalar approach. *Earth and Environmental Science* 26, 1-22.
- Gong, C., Zeng, G., Ge, L., Tan, C., Luo, Q., Liu, X. & Chen, M. (2013). Design of long-distance and high-accuracy rail subgrade deformation monitoring system based on Zigbee wireless network. In: Kim, Y. H. & Yarlagadda, P. (eds.) *Sensors, Measurement and Intelligent Materials*, Pts 1-4.
- Gunn, D.A., Jackson, P.D., Entwisle, D.C., Armstrong, R.W. and Culshaw, M.G. (2003). Predicting subgrade shear modulus from existing ground models. *NDT&E Int.* 36, (3), pp 135 – 144.
- Gunn, D.A. et al. 2006. Assessment of railway embankment stiffness using continuous surface waves. *Proc. 1st Int. Conf. Railway Foundations*, Birmingham, September 2006, pp94-106.
- Gunn, D.A. et al. 2011. Embankment stiffness characterisation using MASW and CSW methods, *Proc. 11th Int. Conf. Railway Engineering*, London, 2011.

- Gunn D.A., Williams, G., Raines, M.G., Busby, J.P., Williams, J.D.O. & Pearson, S.G. 2012. Comparison of surface wave techniques to estimate shear wave velocity in a sand and gravel sequence: Holme-Pierrepoint, Nottingham, UK. *QJEGH*, **45**, pp. 139-160.
- Gunn, D.A. *et al.* 2013. Void detection using surface wave surveys. *Proc. 12th Int. Conf. Railway Engineering*, London.
- Gunn, D.A. *et al.* 2015a. Moisture monitoring in clay embankments using electrical resistivity tomography. *Construction & Building Materials*. (92), 82-94
- Gunn, D.A. *et al.* 2015b. Earthworks ground model development using surface wave surveys. *Proc. XVI ECSMGE*, Edinburgh, 13-17 Sept 2015.
- Gunn, D. *et al.* 2016. Aged embankment characterisation using non-invasive geophysics. *ISSHMII Proc. 7th Int. Conf. on Structural Health Monitoring*, Belfast, 26-27th May, 2016
- Hardin, B.O. & Richart, F.E. 1963. Elastic wave velocities in granular soils. *J. Soil Mech. & Foundations Div.*, 89, (SM1), 33-65
- Hight, D.W., Bennell, J.D., Chana, B., Davis, P.D., Jardine, R.J. and Porovic, E. (1997). Wave velocity and stiffness measurements of Crag and Lower London Tertiaries at Sizewell. *Geotechnique*, **47**, (3), pp 451 – 474.
- Hobbs, P. R. N. *et al.* (2012). Engineering Geology of British Rocks and Soils - Lias Group. British Geological Survey Internal Report, OR/12/032. 323p
- Hugenholtz, C., Walker, J., Brown, O., And Myshak, S. (2015). Earthwork volumetrics with an unmanned aerial vehicle and softcopy photogrammetry. *Journal of Surveying Engineering*, 141, (1): 06014003.
- Joh, S.H. (1996). Advances in the data interpretation technique for spectral analysis of surface waves measurements. Ph.D. Thesis. University of Texas, USA. 240p.
- Jones, R.B. (1958). In-situ measurement of the dynamic properties of soil by vibration methods. *Geotechnique*, vol. 8 (1), pp. 1-21.
- Kane WF, Beck TJ, Hughes JJ (2001) Applications of time domain reflectometry to landslide and slope monitoring. Second Int Symp Work Time Domain Reflectometry Innov Geotech Appl Infrastruct Technol Inst Northwest Univ Evanston, 305–314.
- Lehmann, P., Gambazzi, F., Suski, B., Baron, L., Askarinejad, A., Springman, S.M., Holliger, K., Or, D. (2013). Evolution of soil wetting patterns preceding a hydrologically induced landslide inferred from electrical resistivity survey and point measurements of volumetric water content and pore water pressure. *Water Resources Research*, 49(12), 7992–8004.
- Leicestershire County Council (see <http://www.railwayarchive.org.uk/>)
- Mazzanti, P. 2012. Remote monitoring for deformation. An overview of the seven methods described in previous GINs. *Geotechnical News*, 30(4), 24.
- Menzies, B.K. (2001) Near-surface site characterisation by ground stiffness profiling using surface wave geophysics. Instrumentation in Geotechnical Engineering. H.C.Verma Commemorative Volume. Eds. K.R. Saxena and V.M. Sharma. Oxford & IBH Publishing Co. Pvt. Ltd., New Delhi, Calcutta. pp 43-71.

- Moxhay, AL, Tinsley, RD & Sutton, JA (2001). Monitoring of soil stiffness during ground improvement using seismic surface waves. *Ground Eng.* Jan. 2001, 34-37
- Moxhay, AL, Tinsley, RD, Redgers, RD & Gravell, DC (2008). The prediction of ground settlement from continuous surface wave data. *Ground Eng.* Sept. 2008, 34-38
- Millis SW, Ho ANL, Chan EKK, Lau KWK and Sun HW (2008). Instrumentation and real-time monitoring of slope movement in Hong Kong. The 12th international conference of international association for computer methods and advances in geomechanics (IACMAG). pp. 4563–4570
- Park, C. B., Miller, R. D., Xia, J., 1999. Multichannel Analysis of surface waves (MASW): *Geophysics*, 64, (3), pp. 800-808.
- Perry, J.G. et al. 2003. Infrastructure embankments – condition appraisal and remedial treatment. CIRIA Publ. C592. 245p
- Raines, M.G., D.A. Gunn, Morgan, D.J.R., Williams, G. and Williams, J.D.O. & Caunt, S., 2011. Refraction microtremor (ReMi) to determine the shear wave velocity structure about a mineshaft. *Q.J.E.G.H.* 44, pp 211-220.
- Reeves, G.M., Sims, I. & Cripps, J.C. 2006. Clay materials used in construction. *Geol. Soc. Eng. Geol. Sp. Publ.* 21. London, 525p.
- Richart F.E. Jr., Wood R.D. & Hall J.R. Jr. (1970). *Vibration of soils and foundations*. Prentice-Hall, New Jersey. 414p
- Ridley, A.M., Dineen, K., Burland, J.B. and Vaughan, P.R. (2003) Soil matrix suction: some examples of its measurement and application in geotechnical engineering. *Géotechnique* 53, No.2, pp241 – 254.
- Rix, G.J. (1988). Experimental study of factors affecting the spectral analysis of surface waves method. Ph.D. Thesis, University of Texas, USA.
- Rucker, M. L. 2003. Applying the refraction microtremor (ReMi) shear wave technique to geotechnical characterisation. Proc. 3rd Int. Conf. Application of Geophysical Methodologies and NDT to Transportation and Infrastructure, December 8-12, 2003, Orlando, Florida, USA.
- Scaioni M, Longoni L, Melillo V, Papini M (2014) Remote Sensing for Landslide Investigations: An Overview of Recent Achievements and Perspectives. *Remote Sens* 6:1 – 26.
- Selig, E.T. & Waters, J.W., 1994. Rail geotechnology and substructure management. Thomas Telford Ltd., London. 446p
- Skempton, A.W., 1996. Embankments and cuttings on the early railways. *Construction History*, 11: 33-39.
- Smethurst, J. A., Clarke, D. and Powrie, W. (2012) Factors controlling the seasonal variation in soil water content and pore water pressures within a lightly vegetated clay slope. *Géotechnique*, 62, (5), 429-446.
- Smith A, Dixon N (2015) Quantification of landslide velocity from active waveguide-generated acoustic emission. *Can Geotech J* 52:413–425.

- Socco, L.V., C. Strobbia, 2004, Surface-wave method for near-surface characterization: a tutorial: *Near Surface Geophysics* 2(4), 165-185
- Steelman CM, Endres AL, Jones JP (2012) High-resolution ground-penetrating radar monitoring of soil moisture dynamics: Field results, interpretation, and comparison with unsaturated flow model. *Water Resour Res* 48:1–17.
- Stevenson, D., 1886. *The principles and practice of canal and river engineering*. 3rd Ed. Edinburgh University Press, 406p.
- Toll DG, Lourenço SDN, Mendes J (2013) Advances in suction measurements using high suction tensiometers. *Eng Geol* 165:29–37.
- Topp C, Davis JL, Annan AP (1980) Electromagnetic Determination of Soil Water Content: Measurements in Coaxial Transmission Lines. *Water Resour Res* 16:574–582.
- Viggiani G & Atkinson J.H., 1995. Stiffness of fine grained soil at very small strains. *Geotechnique*, 45, (2), 249-265.
- Wang E F, Wang G, Zhang Y M, Huo Z T, Peng X M, Araiba K, Takeuchi A (2008). Displacement monitoring on Shuping landslide in the Three Gorges Dam Reservoir area, China from August 2004 to July 2007. *Landslides and Engineered Slopes*, Chen et al (Eds.), Taylor and Francis, London. Vol. 2, pp. 1321 – 1327.
- Whalley, WR, Jenkins, M & Attenborough (2012). The velocity of shear waves in unsaturated soil. *Soil & Tillage Res.* 125, 30-37.
- Woodward, P.K, Laghrouche, O., El-Kacimi, A., Medero, G., Banimahd, M., Kennedy, J., Connolly, D., Giannopoulos, A., & Forde, M.C., High-speed Rail Geotechnical Issues. *Proc. 11th Int. Conf. Railway Engineering*, London, 2011.
- Xia J., Miller R.D. and Park C.B. 1999. Estimation of near-surface shear-wave velocity by inversion of Rayleigh waves. *Geophysics* 64,691–700.
- Zagyapan, M. and Fairfield, C.A. (2000). The use of continuous surface wave and impact techniques to measure the stiffness and density of trackbed materials. *Proc. 3rd Int. Conf. Railway Engineering*, London.

Figure captions (images as individual files separate to your MS Word text file).

Figure 1. Map of England & Wales showing location of case study sites.

Figure 2. Field source and receiver configurations used in surface wave surveys.

- a. Field curves from two receivers used to calculate phase velocity in the steady state Rayleigh method, (modified from Rix 1988).
- b. Velocity from phase measurements at fixed frequencies on small number of receivers in the CSW method.
- c. Velocities across geophone arrays over a range of frequencies calculated in the MASW method.
- d. Hammer and plate source and towed streamer use for MASW surveys.

Figure 3. Overview of surface wave processing scheme from field coverage to the generation ground model images.

- a. Relative positions of 1D profiles via roll-along or towed procedures used to generate 2D sections.
- b. Field record showing refracted and Rayleigh wave: 8-channel group selected from Rayleigh wave used to construct dispersion curve and velocity profile.
- c. Phase velocity – frequency transform for 8-channel group: Rayleigh wave picked from high intensity low velocity feature.
- d. Factored S-wave phase velocity-depth profile plotted at group mid-point: Depth equivalent to $1/3$ wavelength.

Figure 4. Ground model constructed from CSW and MASW surveys at embankment along Great Central Railway.

- a. Field map of embankment showing location of MASW survey lines and CSW profile points.
- b. Stiffness section showing interface between fine and coarse fill grades.

Figure 5. Anatomical visualisation of embankment end-tip structure via de-construction of a 3D ground stiffness model.

Figure 6. Surface wave surveys at embankment along Knottingley and Goole canal near Eggborough.

- a. Location of the model section relative to cavity, embankment axis and positions of geophone line arrays.
- b. Subsurface structure visualised via 3D shear wave velocity model.

Figure 7. Void associated with very low velocity zones in 3D ground shear wave velocity model.

- a. Extent of void highlighted using selected iso-volume velocity ranges.
- b. Fence panels show small trough structure through which water flowed from canal into void.

Figure 8. MASW survey at the Laverton embankment along the Gloucester-Warwickshire Railway.

- a. Layout of survey line relative to CPT profile locations.
- b. 2D section of shear wave velocity profile along axis of embankment.

Figure 9. Photograph of wall and floor of pit at CPT3.

Figure 10. Geotechnical properties through Laverton embankment section near CPT 3.

- a. 2D cross-section showing CPT penetration resistance.
- b. Moisture content and bulk density profiles from core taken beneath embankment crest

Figure 11. Embankment velocities relative to 2014 temperature and rainfall sequence. (After Bergamo *et al.* 2016.)

Tables

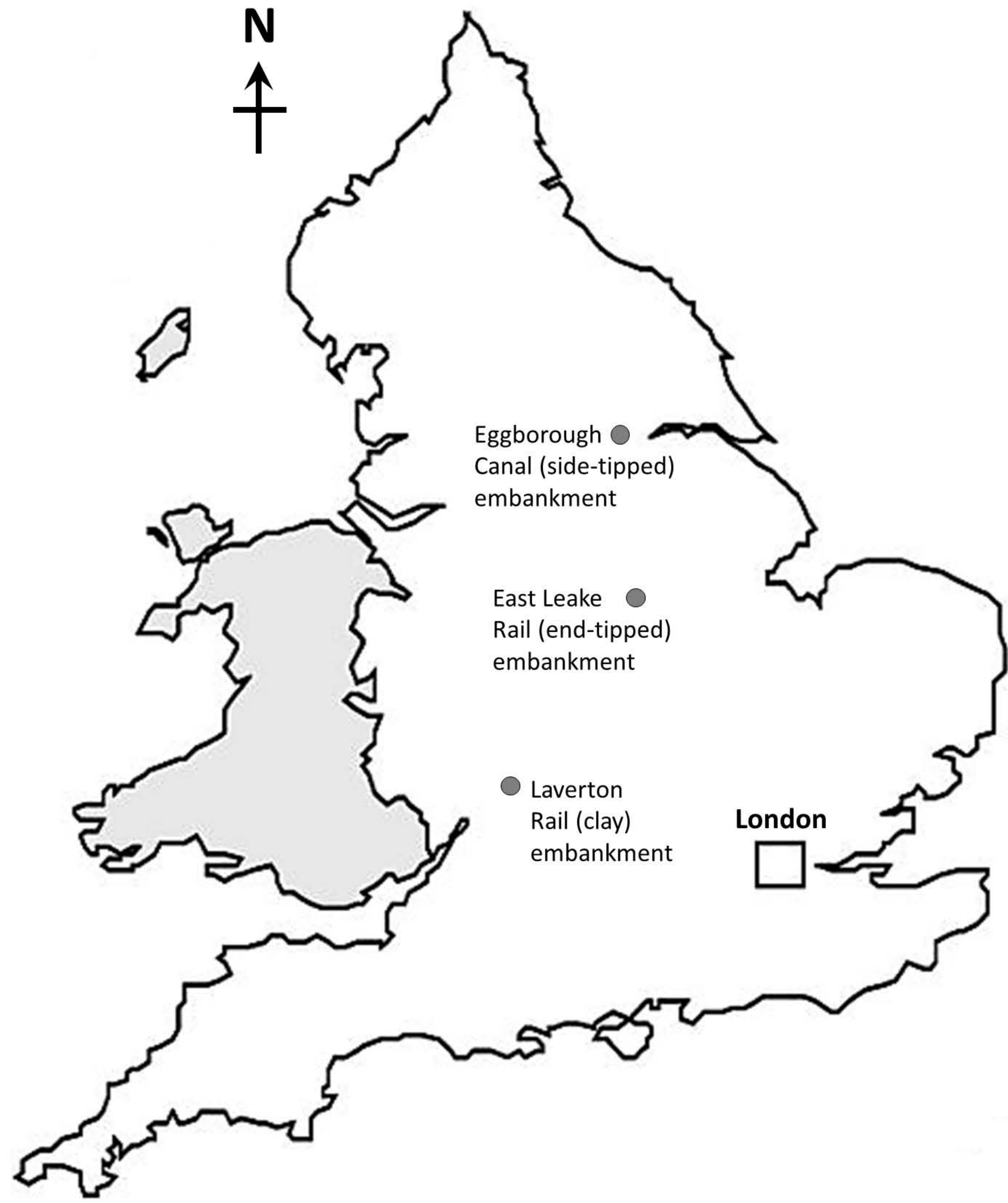
Table 1. Geotechnical properties of Charmouth Mudstone measured on samples taken from the Laverton embankment and outcrops within the Worcester Basin.

Reworked Charmouth Mudstone from embankment samples (6 no. off)		
Mean Bulk Density: 1.92 Mg.m ⁻³	Plastic Limit Range	Liquid Limit Range
Moisture Content: Range: 23 - 33% Mean: 26 %	27 - 37%	61 - 77%
Triaxial Tests at Effective Stress	Drained Cohesion, c'	Drained Friction Angle ϕ'
East Flank (upper 0.5 m)	11.3 kPa	19.3 °
West Flank (upper 0.5 m)	7.3 kPa	16.2 °
Median values for Charmouth Mudstone in Worcester Basin from Hobbs <i>et al.</i> (2012)		
(no. off samples stated)		
Index Test Values (>100 samples)	BS 1377 : Pt2 : 1990	
Bulk Density: 2.03 Mg.m ⁻³	Plastic Limit	Liquid Limit
Natural in situ Moisture Content: 22%	23%	53%
Triaxial Tests at Effective Stress	BS 1377 : Pt8 : 1990	
	Drained Cohesion, c'	Drained Friction Angle ϕ'
(>10 samples)	19 kPa	26°

Residual Values	Drained Cohesion, c_r'	Drained Friction Angle ϕ_r'
	9 kPa	14°

Table 2. Common asset monitoring approaches: Surface and subsurface methods mapped onto preventative – responsive spectrum.

Condition Timeline		As Built	Serviceable	Marginal	Poor	Failure
Management Strategy		Preventative			Responsive	
Actions / Relative Costs		Intervention		Refurbish	Renewal	
Monitoring Approaches		Subsurface Thresholds Precursors			Surface Visual Signs Movement	
Monitoring Parameters		---- Ground Conditions ----			---- Surface Deformation ----	
		---- Subsurface Def ⁿ ----				
Monitoring Methods	Ground Conditions	Point Sensors: Moisture ^{1,2} ; Suction ^{3,4} ; Pore Pressure ^{5,6} ; Wireless Sensor Networks ⁷				
		Non-Invasive Geophysical Imaging: GPR ⁸ ; Resistivity ⁹ ; Seismic ^{10,11} (incl. Surface Waves)				
	Subsurface Deformation	Small Strain (Pre-cursors): Acoustic Emission (ALARMS) ^{12,13}				
		Large Strain: Inclinometers; Shape Arrays ¹⁴				
	Surface Deformation	Remote: Satellite (InSAR) ^{15,16} ; Terrestrial Laser; Robot Tot. St. ¹⁶ ; Photogrammetry ¹⁷ (UAV ¹⁸)				
		Walker: GPS; dGPS ¹⁹				
Ground Installation: Tilt; Extensometer ²⁰						
Exemplars: 1-Topp et al. 1980; 2-Kane et al. 2001; 3-Ridley et al. 2003; 4-Toll et al. 2013; 5-Smethurst et al. 2012; 6-Lehmann et al. 2013; 7-Gong et al. 2013; 8-Steelman et al. 2012; 9-Chambers et al. 2014; 10-Donohue et al. 2013b; 11-Bergamo et al. 2016; 12-Dixon et al. 2015; 13-Smith & Dixon 2015; 14-Abdoun et al. 2013; 15-Scaioni et al. 2014; 16-Mazzanti 2012; 17-Bemis et al. 2014; 18-Hughenolt et al. 2015; 19-Mills et al. 2008; 20-Wang et al. 2008						



N
↑

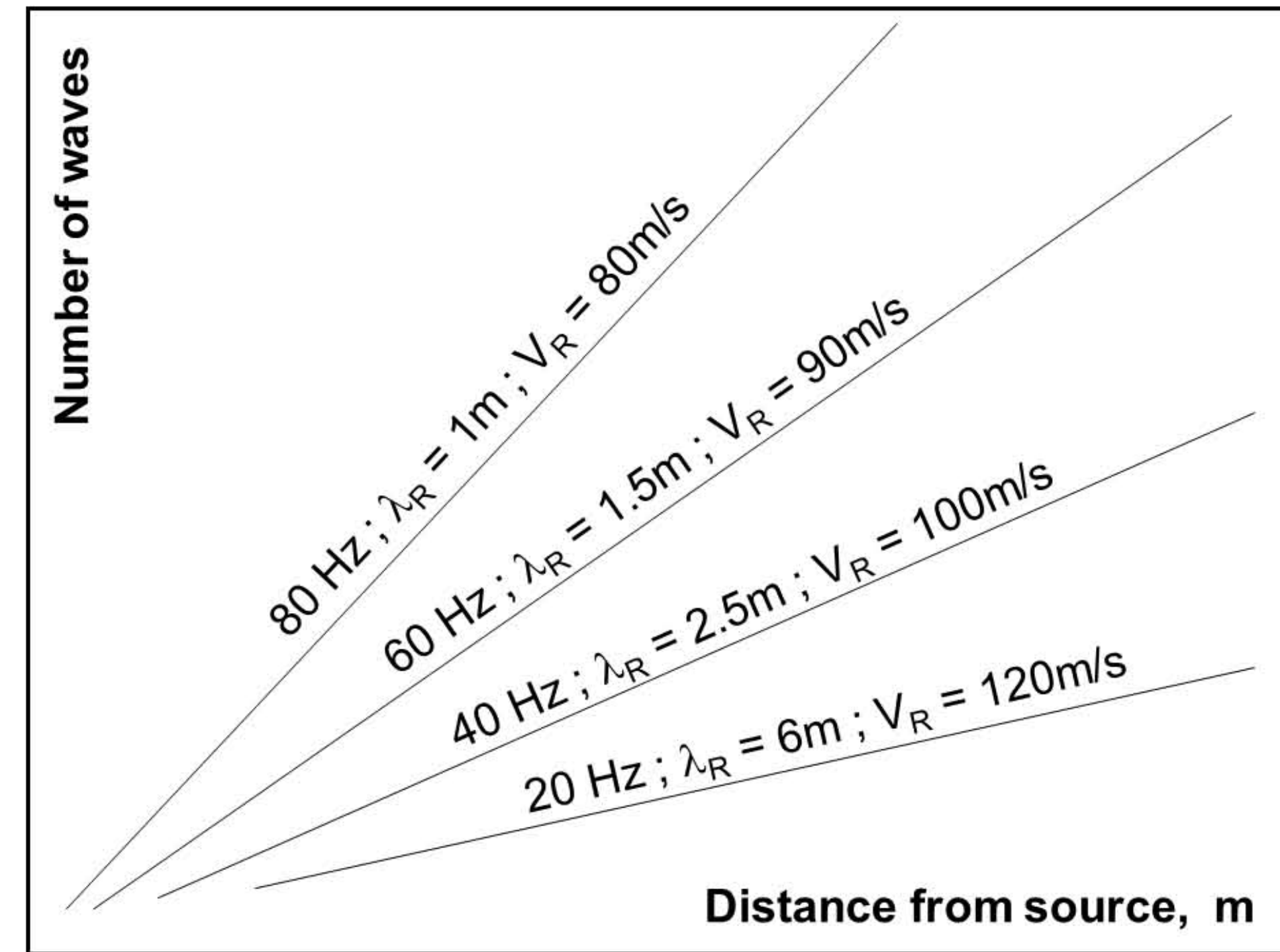
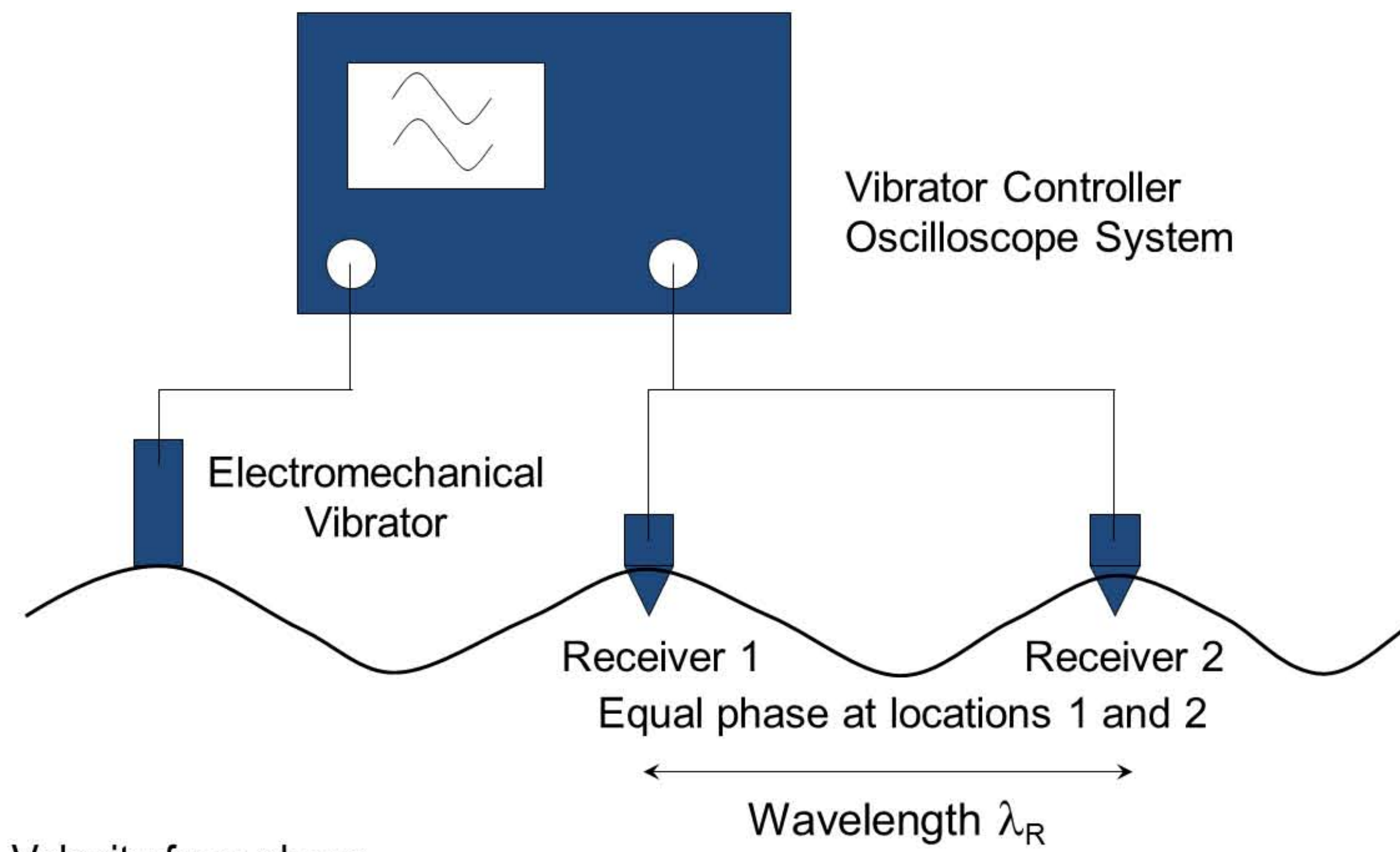
Eggborough ●
Canal (side-tipped)
embankment

East Leake ●
Rail (end-tipped)
embankment

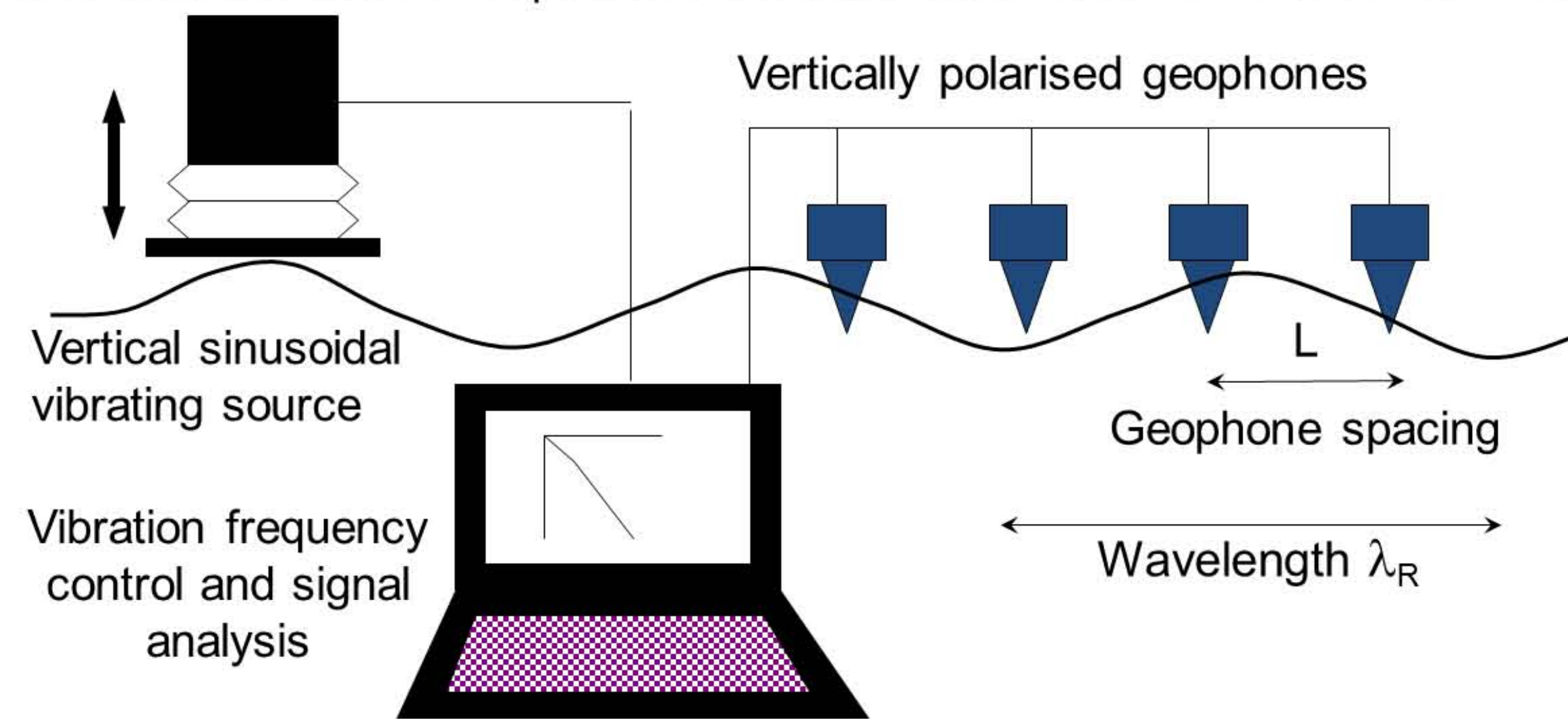
● Laverton
Rail (clay)
embankment

London
□

a. Field curves from two receivers used to calculate phase velocity in the steady state Rayleigh method, (modified from Rix 1988).

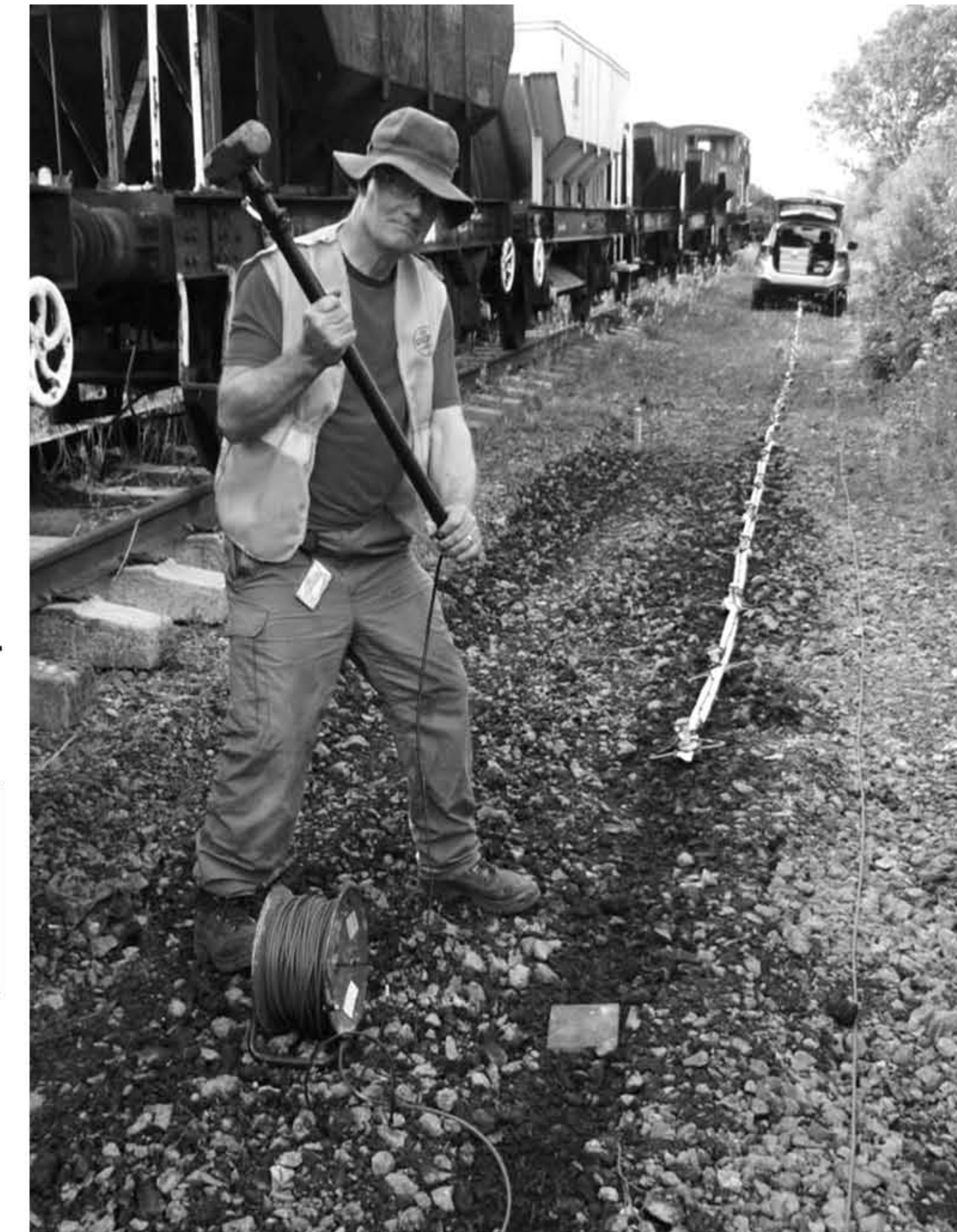
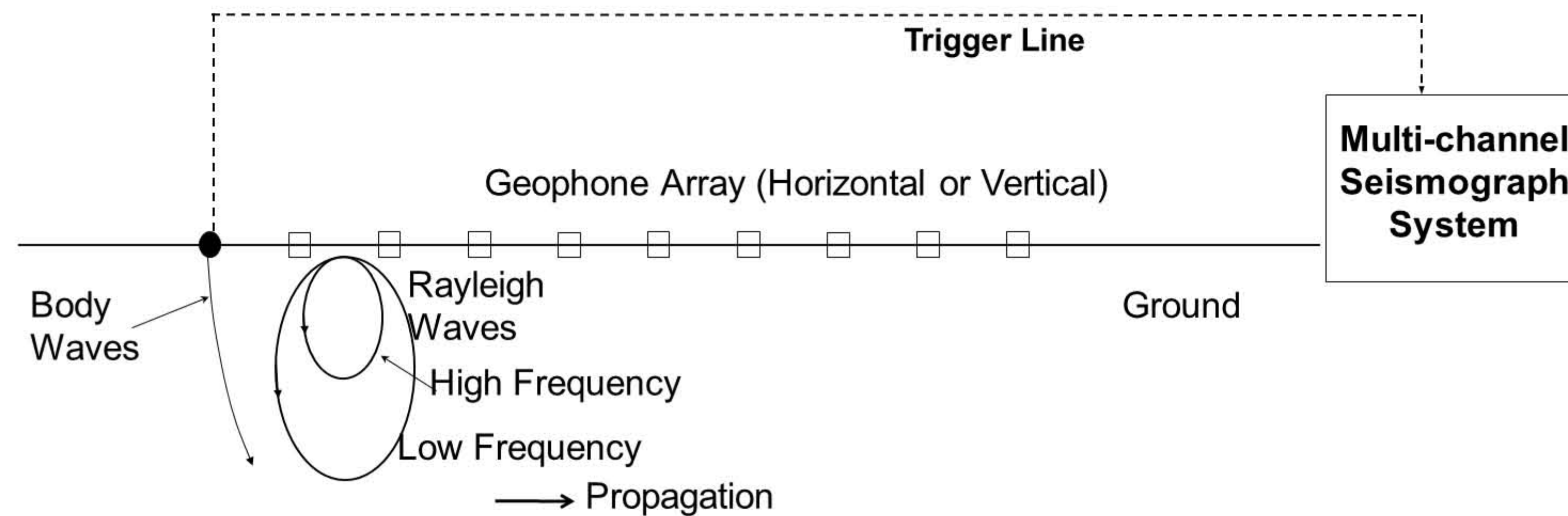


b. Velocity from phase measurements at fixed frequencies on small number of receivers in the CSW method.

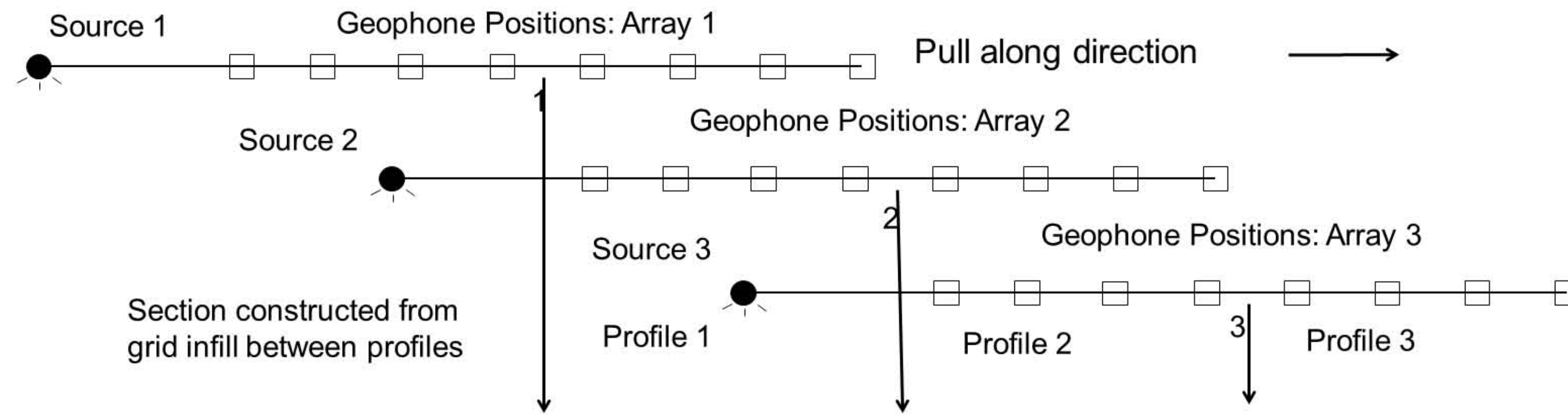


d. Hammer and plate source and towed streamer use for MASW surveys.

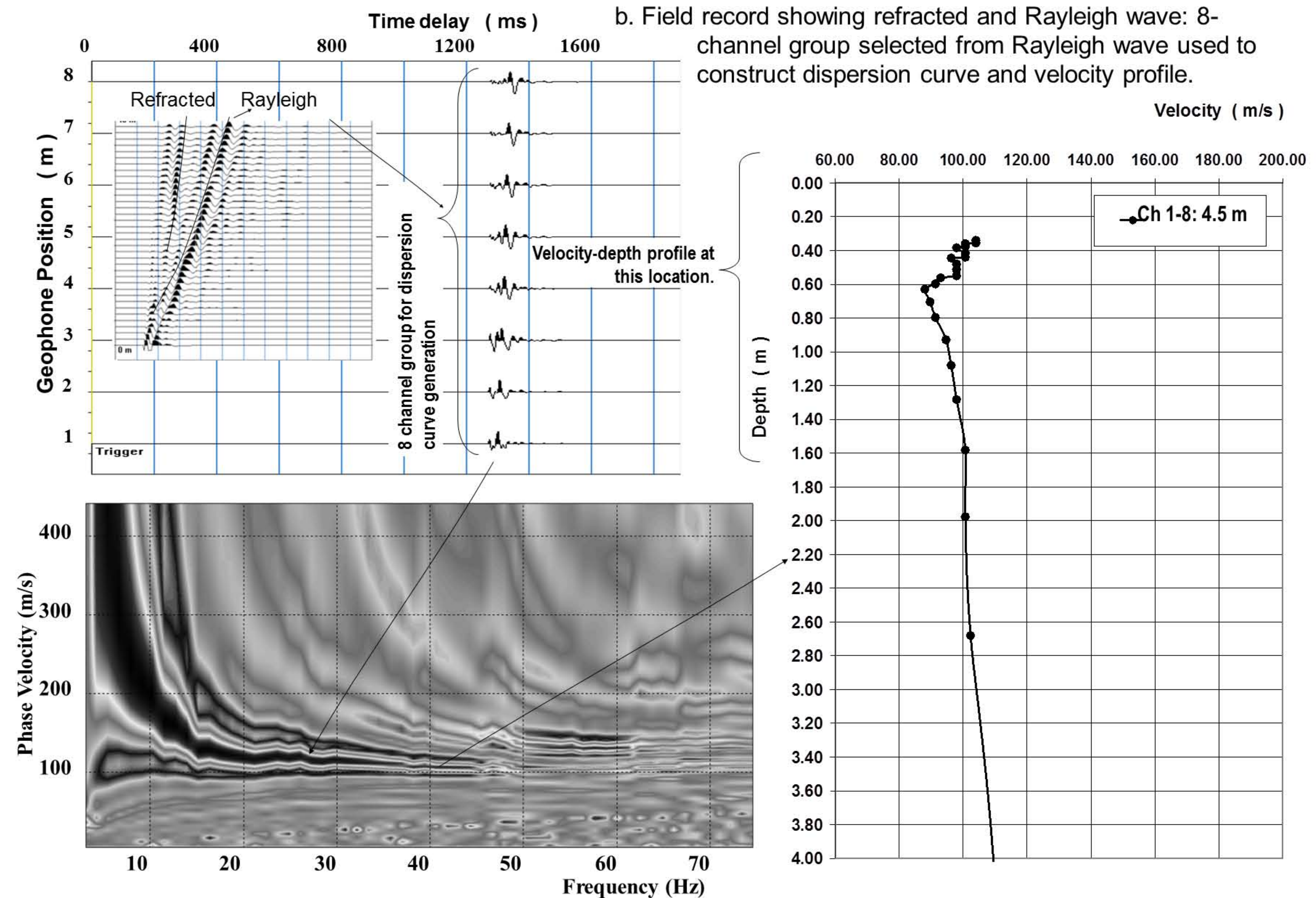
c. Velocities across geophone arrays over a range of frequencies calculated in the MASW method.



a. Relative positions of 1D profiles via roll-along or towed procedures used to generate 2D sections.



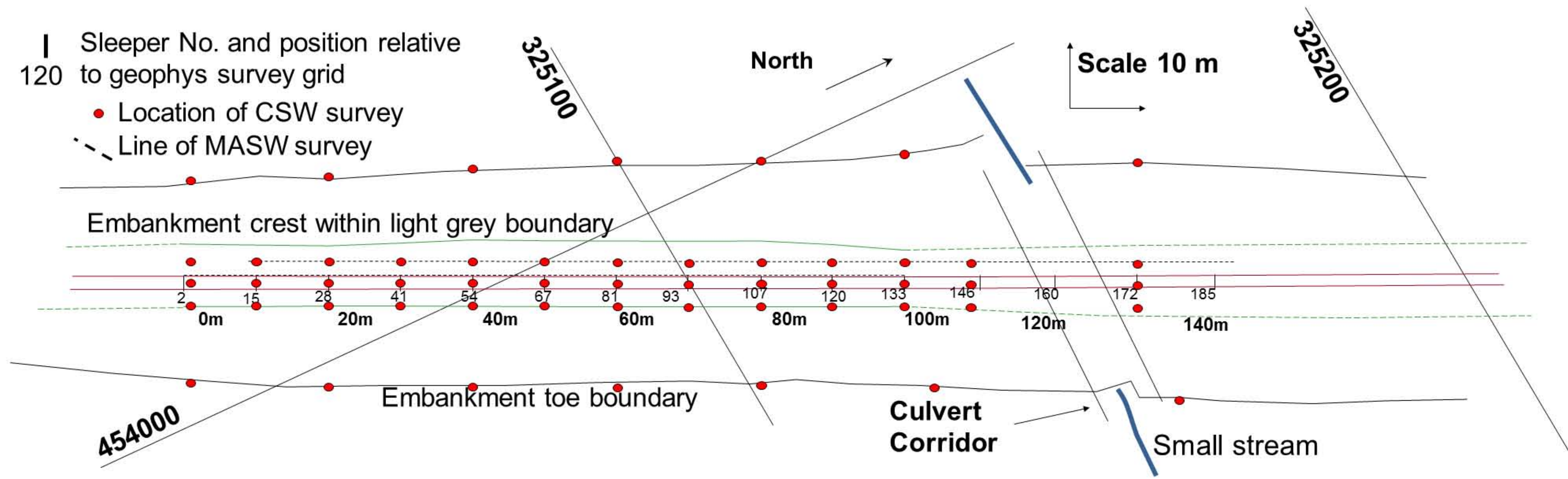
b. Field record showing refracted and Rayleigh wave: 8-channel group selected from Rayleigh wave used to construct dispersion curve and velocity profile.



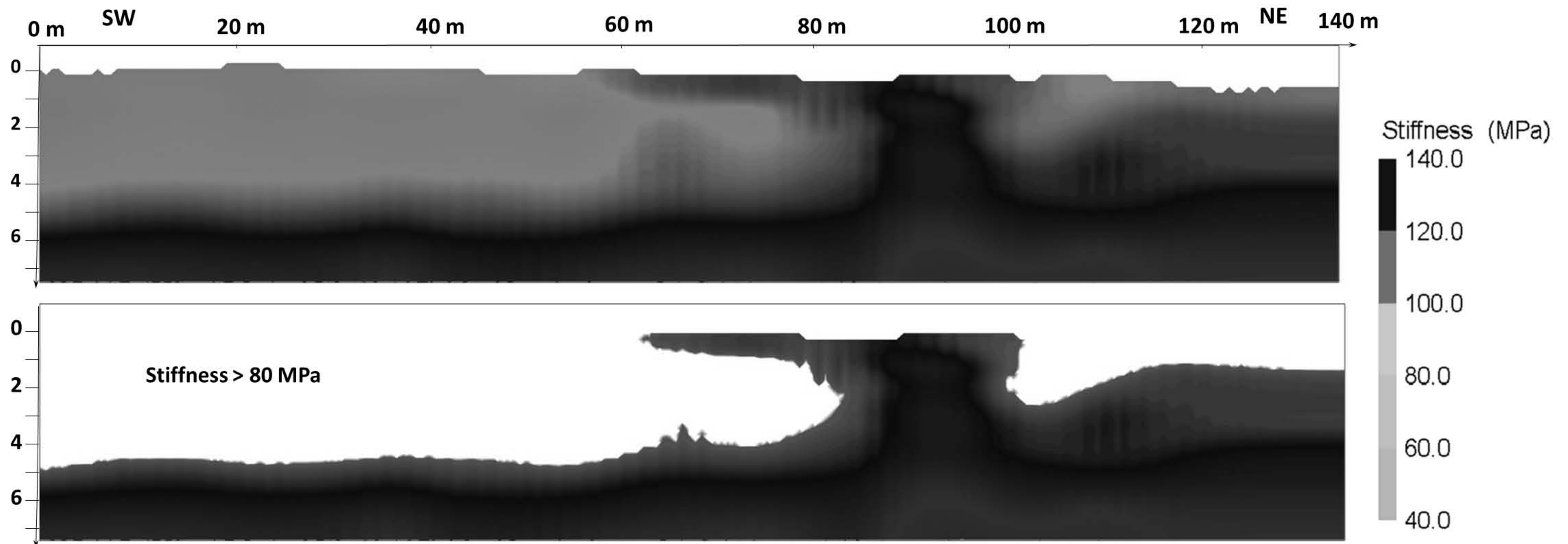
c. Phase velocity – frequency transform for 8-channel group: Rayleigh wave picked at pick intensity of low velocity feature.

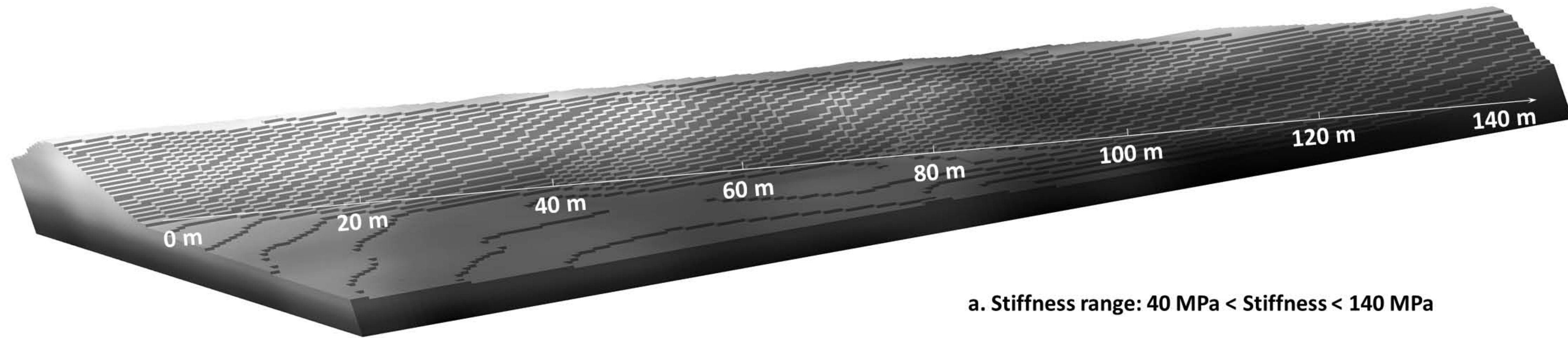
d. Factored S-wave phase velocity-depth profile plotted at group mid-point: Depth equivalent to 1/3 wavelength.

a. CSW profile and MASW survey line locations shown in BNG (co-ordinates in bold).

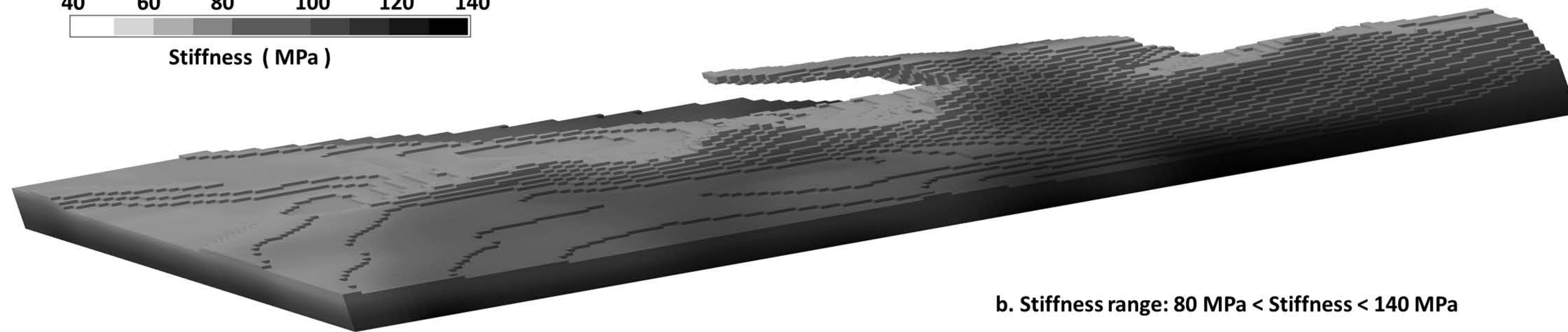


b. Stiffness section modelled from the surface wave survey profile interpretations.



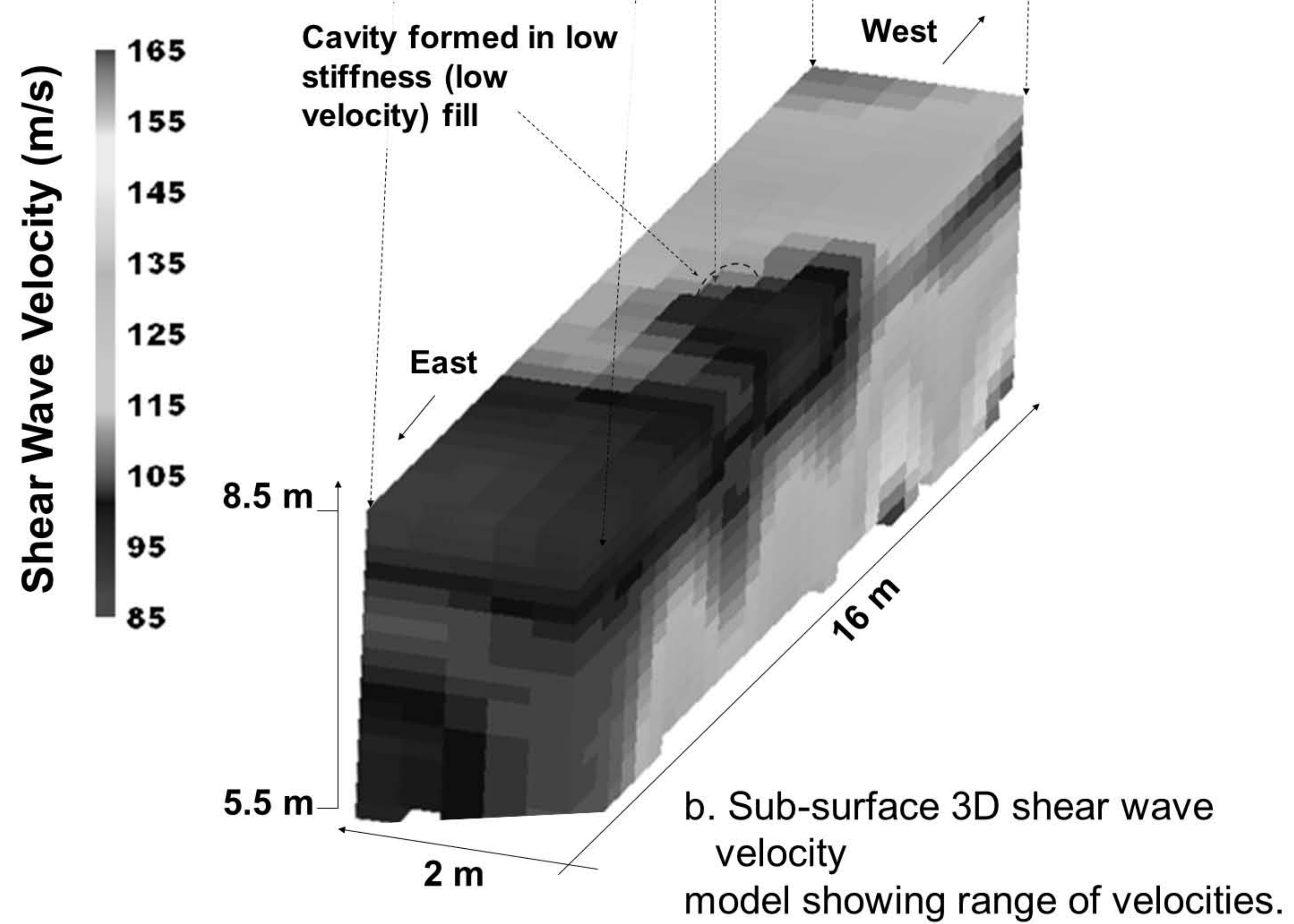
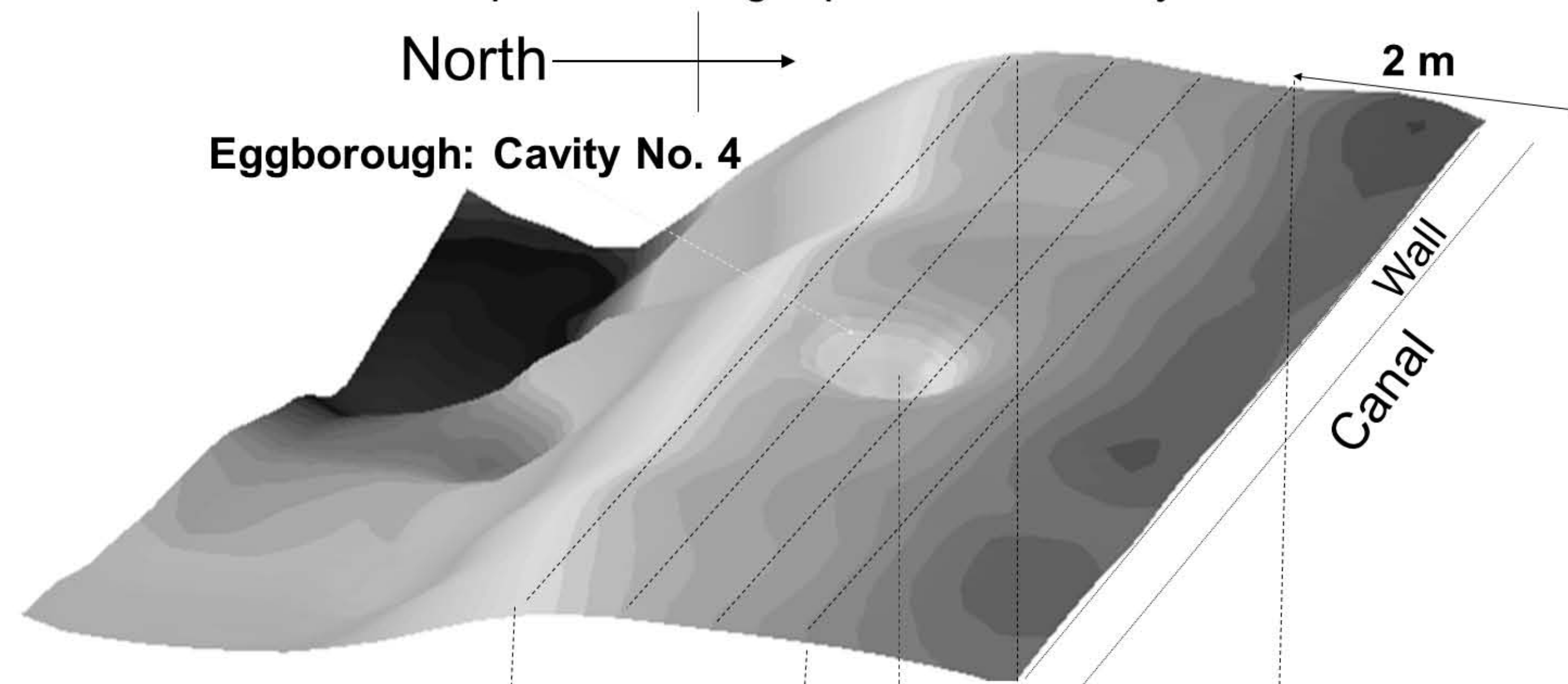


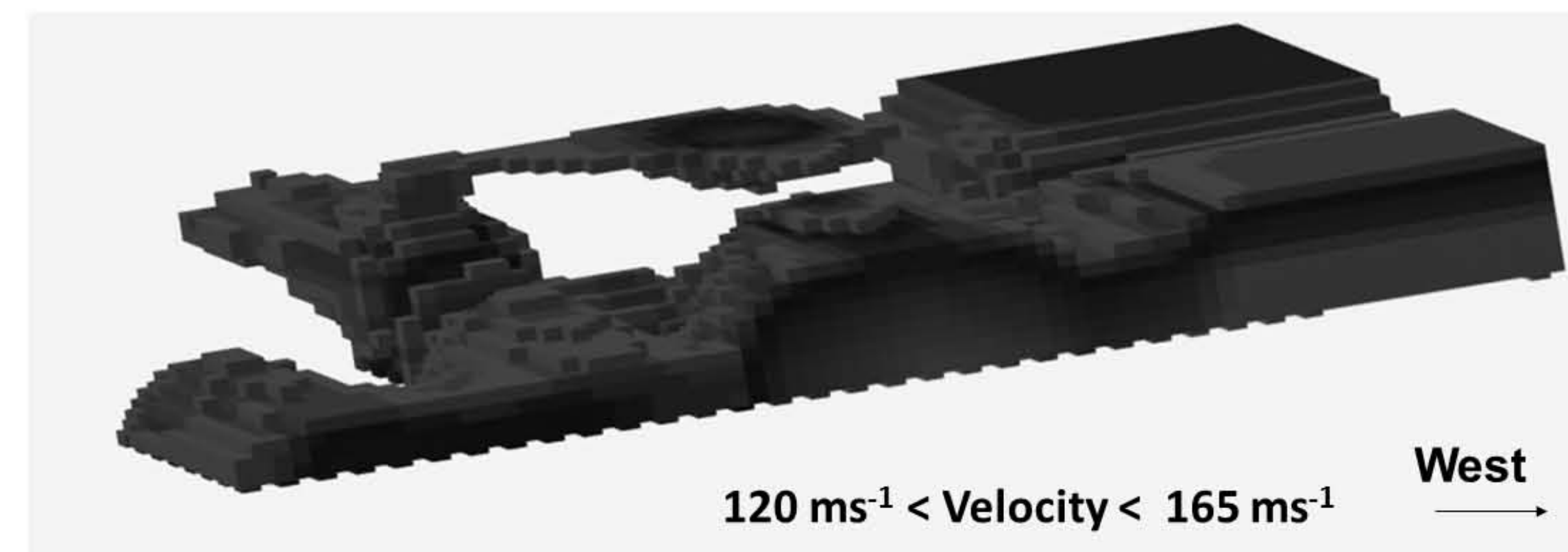
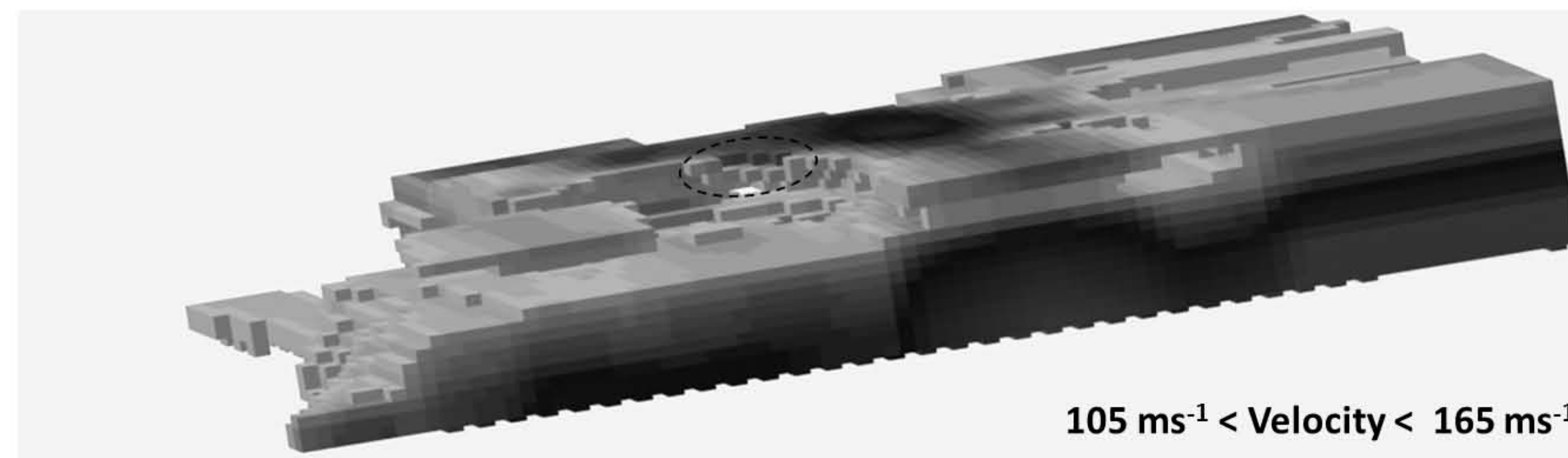
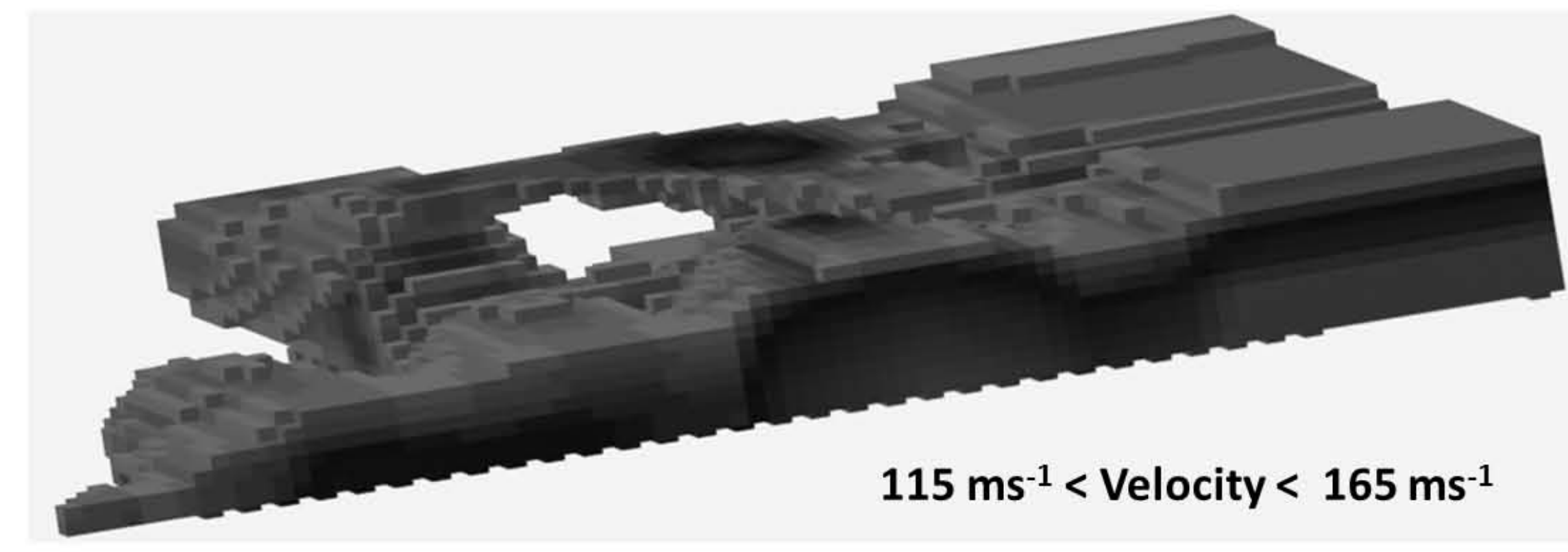
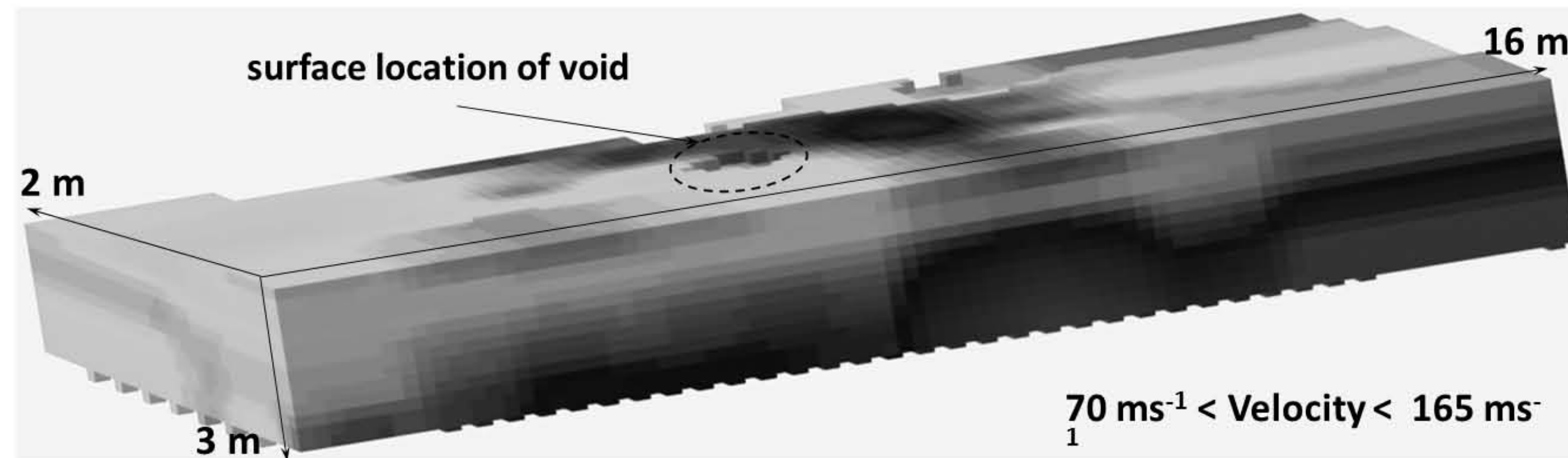
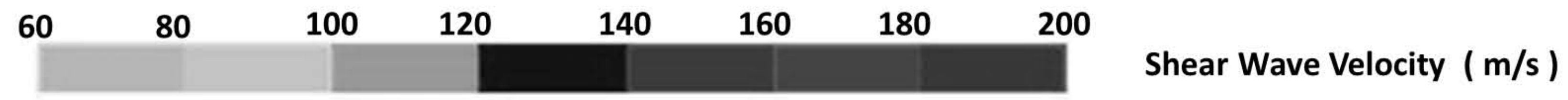
a. Stiffness range: 40 MPa < Stiffness < 140 MPa



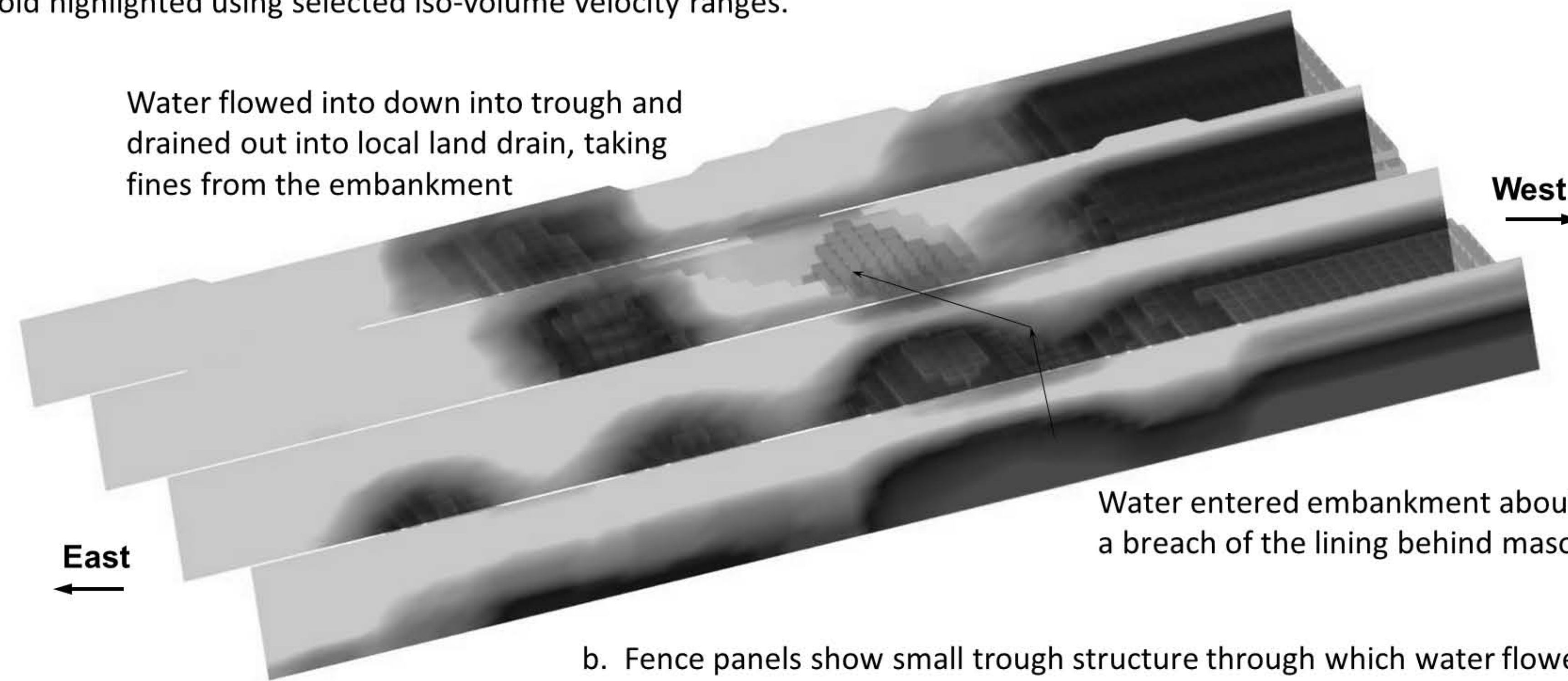
b. Stiffness range: 80 MPa < Stiffness < 140 MPa

a. Location of the model section relative to cavity, embankment axis and positions of geophone line arrays.

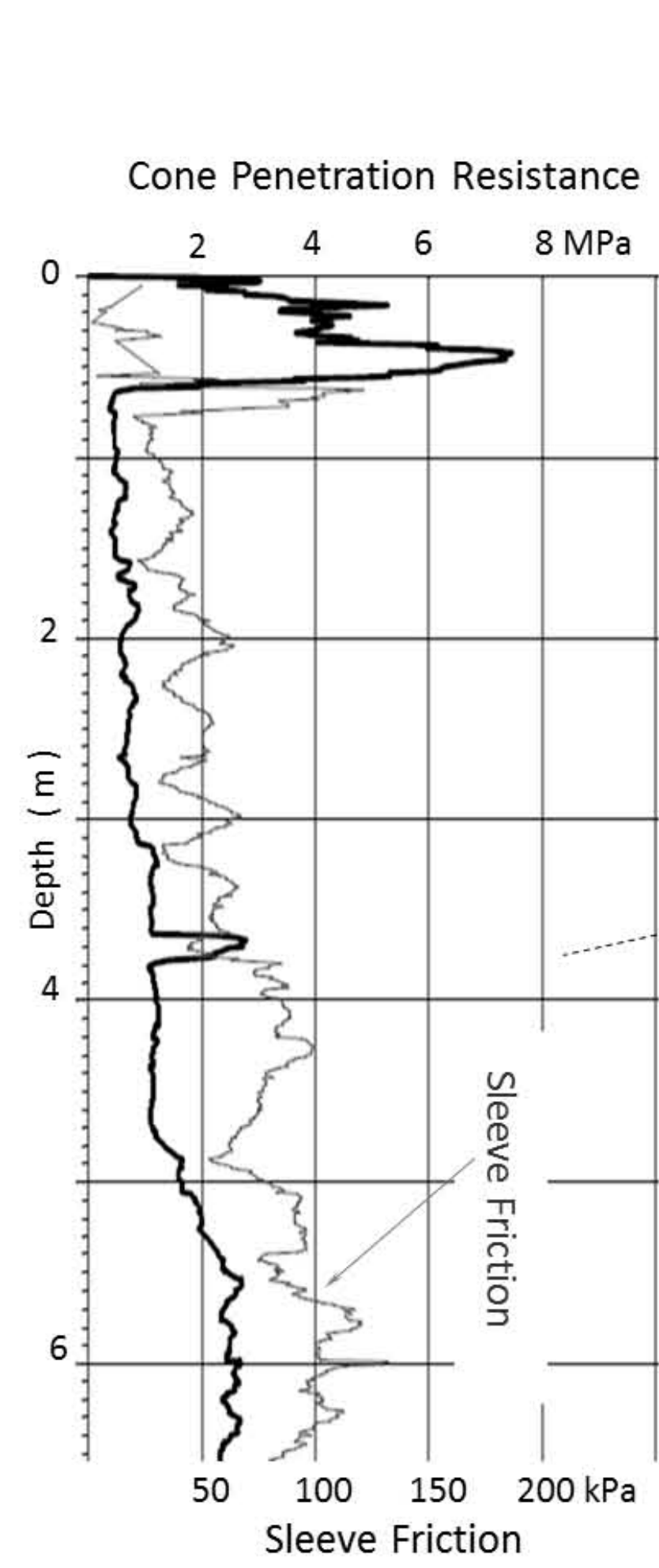




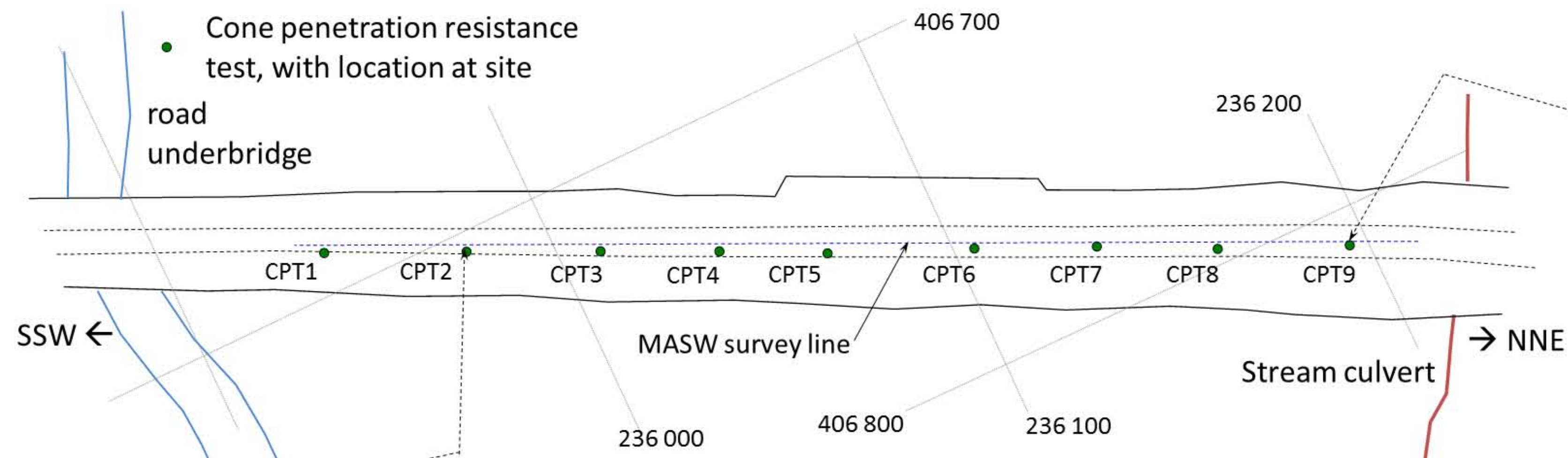
a. Extent of void highlighted using selected iso-volume velocity ranges.



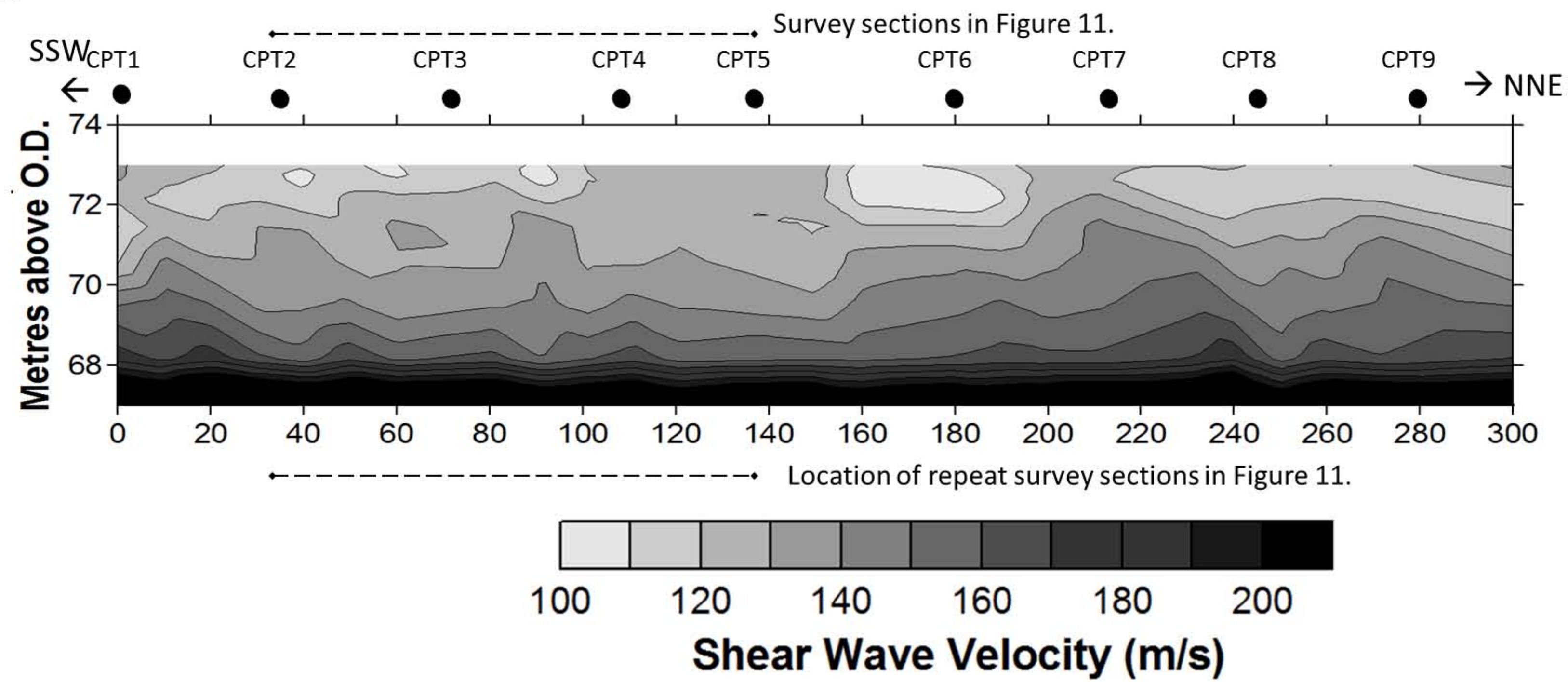
b. Fence panels show small trough structure through which water flowed from canal into void.



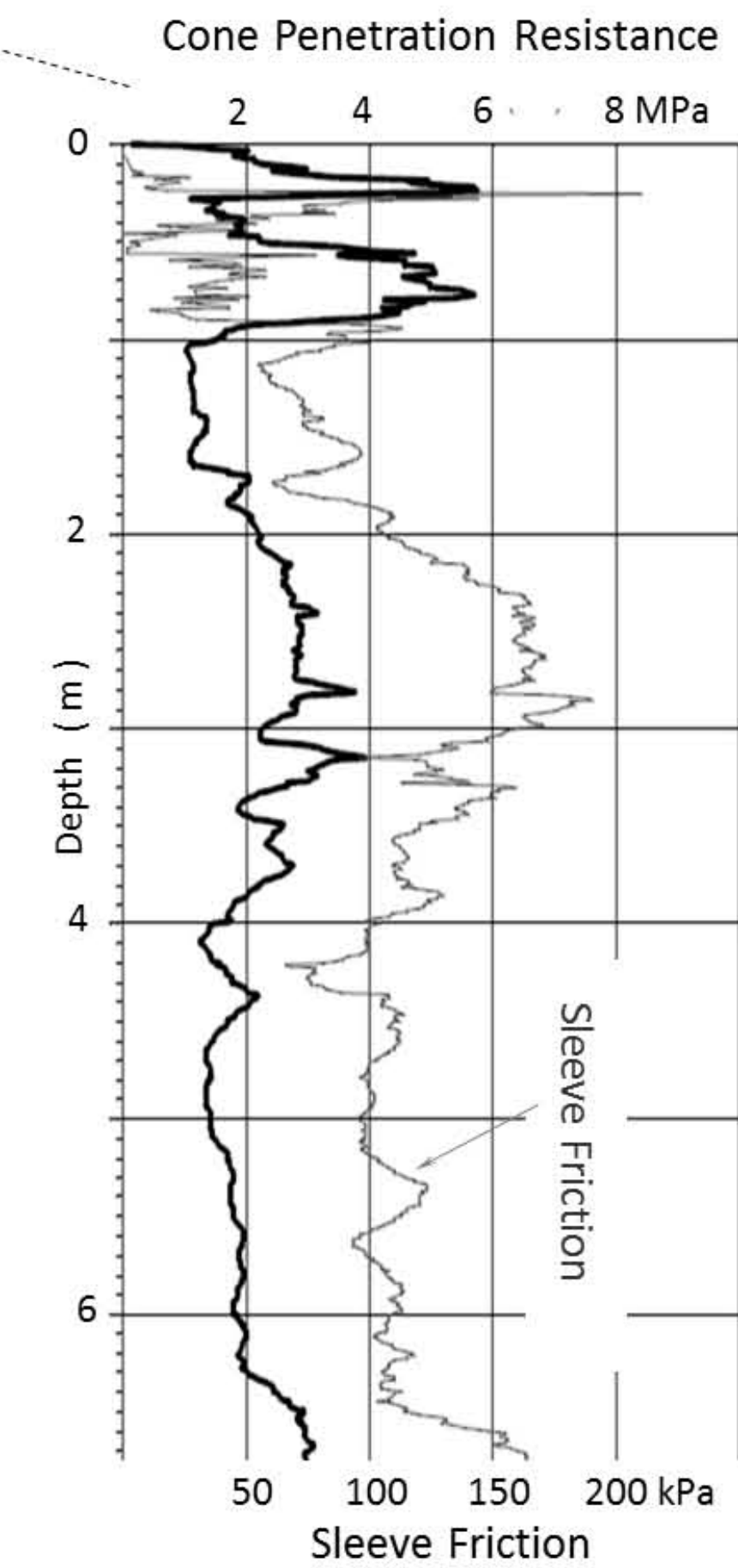
Cone Penetration Test (CPT) at CPT 2



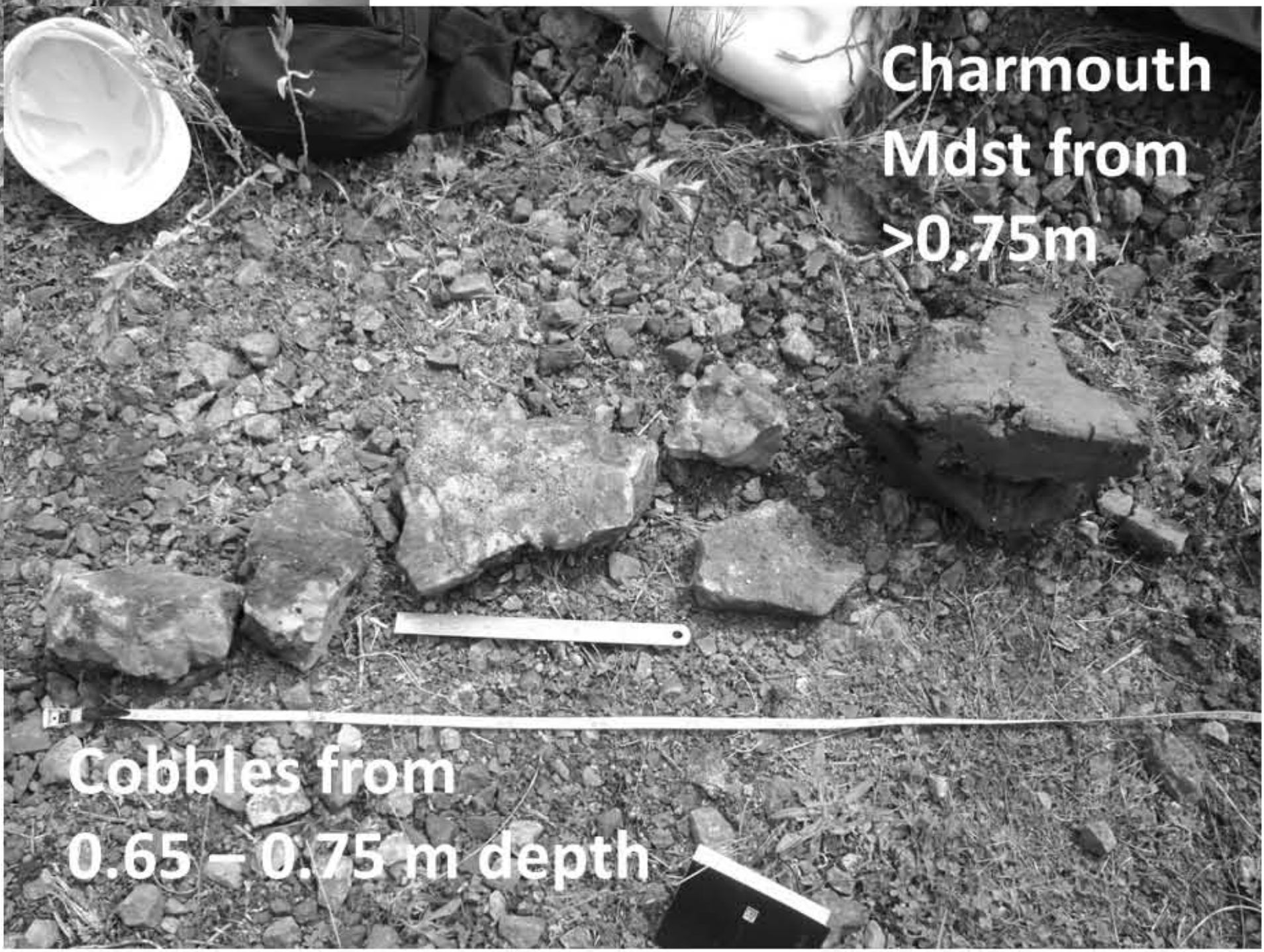
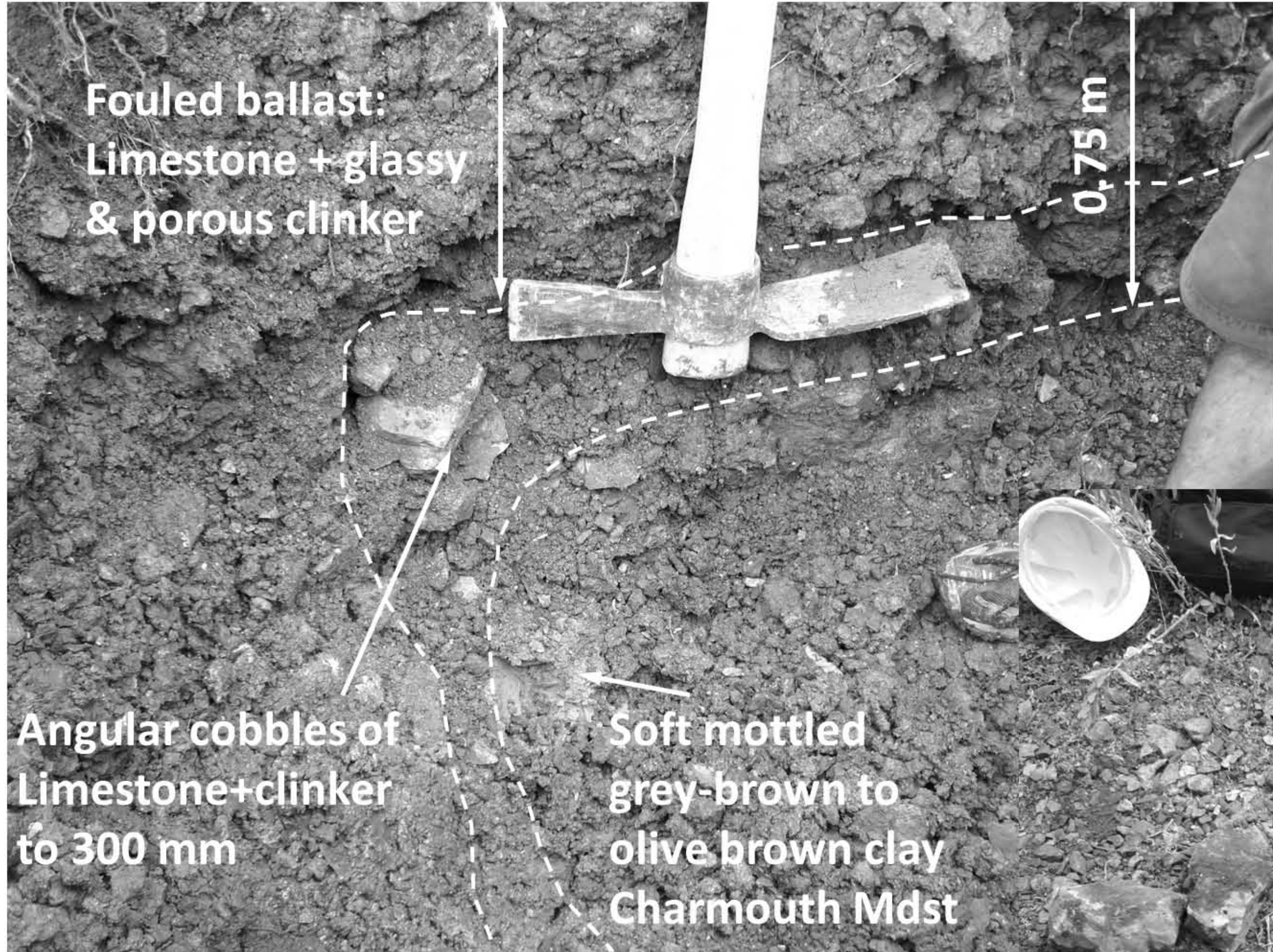
a. Layout of survey line relative to CPT profile locations.



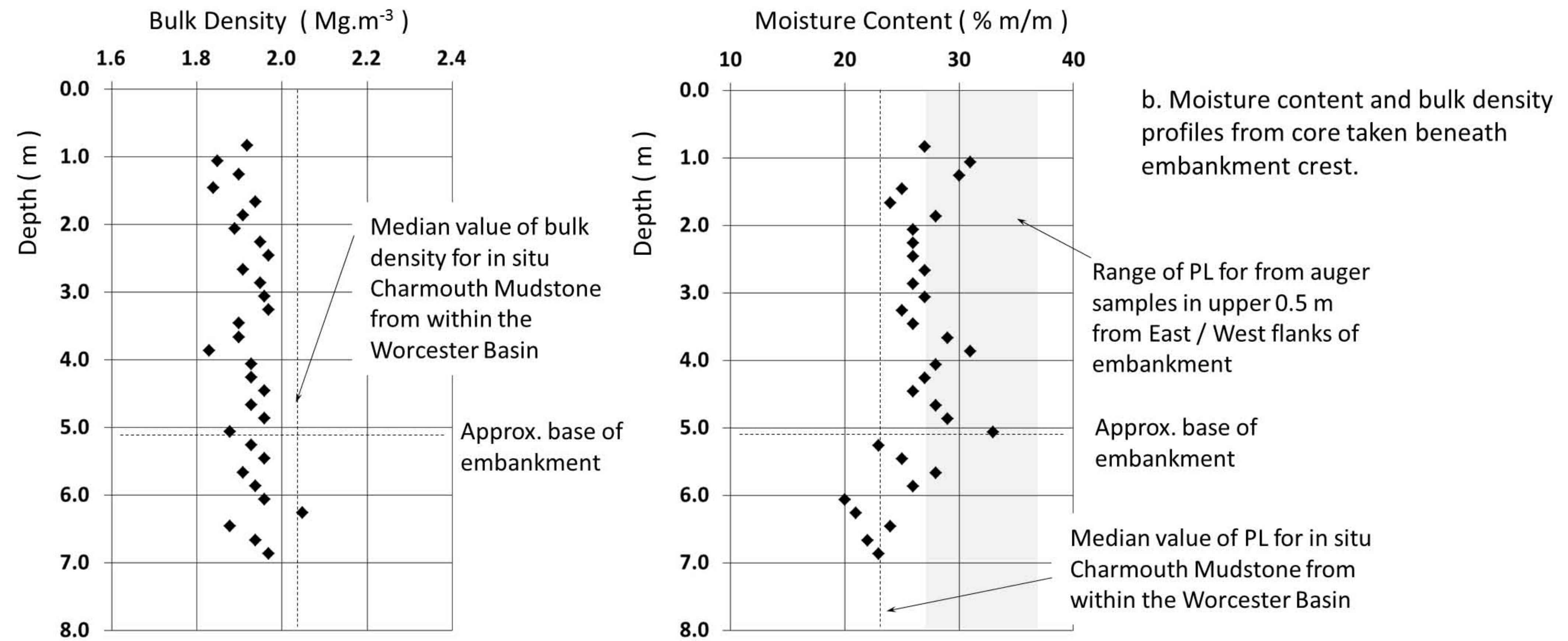
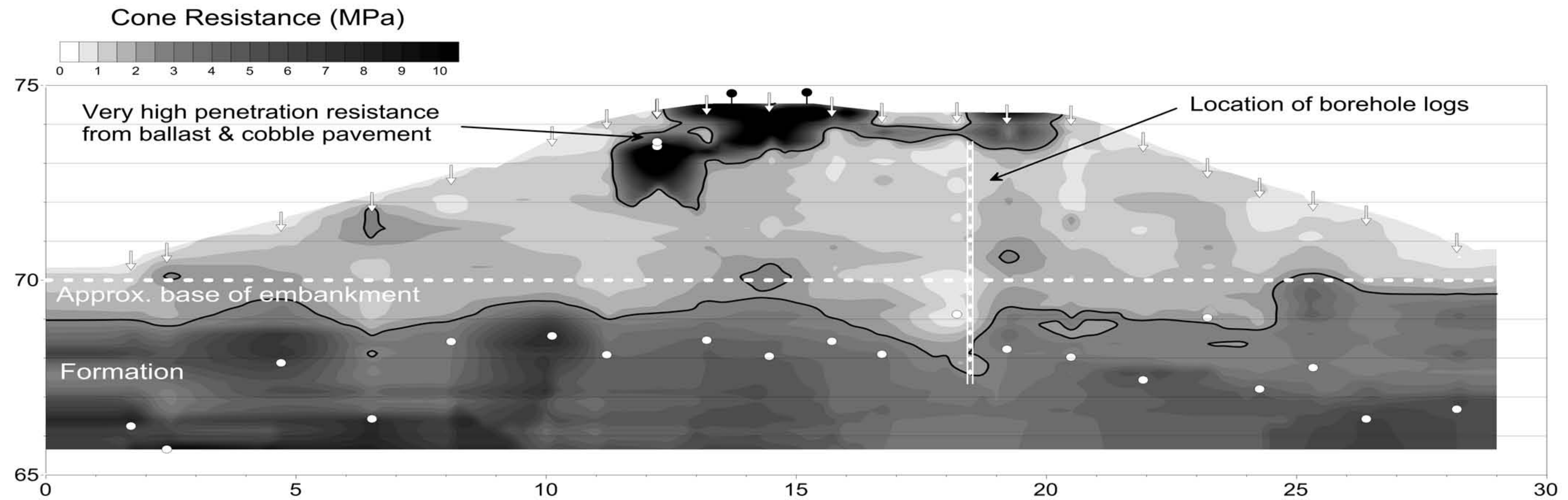
b. 2D section of shear wave velocity profile along axis of embankment.



Cone Penetration Test (CPT) at CPT 9



a. 2D cross-section showing CPT penetration resistance.



b. Moisture content and bulk density profiles from core taken beneath embankment crest.

